Stochastic finite element method for analysis of transport of nonlinearly sorbing solutes in three-dimensional heterogeneous porous media

A. Chaudhuri[1] and M. Sekhar[1]

Received 13 January 2006; revised 2 February 2007; accepted 21 February 2007; published 24 July 2007.

[1] The probabilistic analysis by Monte Carlo simulation method (MCSM) for the transport of nonlinear reactive solutes in a three-dimensional heterogeneous porous medium is a computationally prohibitive task. For linear transport problems, the perturbation-based stochastic finite element method (SFEM) has been found to be computationally efficient with acceptable accuracy. This provides a motivation to develop the SFEM for the nonlinear reactive solute transport. In the present study, SFEM is developed for the transport of equilibrium nonlinear sorbing solutes, which follow the Langmuir-Freundlich isotherm. This method produces a second-order accurate mean and a first-order accurate standard deviation of concentration. In this study, the governing medium propertis viz. hydraulic conductivity, dispersivity, molecular diffusion, porosity, sorption, and decay coefficients are considered to vary randomly in space. The performance of SFEM is compared to MCSM for both one- and three-dimensional transport problems. The mean and the standard deviation of concentration for various test cases obtained with the SFEM compares well for the mild heterogeneity cases (standard deviation of log hydraulic conductivity less than 0.85) tested. SFEM produces a sharp front for the mean and the standard deviation of concentration while fronts obtained by MCSM are found to be dispersive. The error associated with the results obtained by SFEM is sensitive to the boundary conditions, the size of the domain, and the plume size. For a higher nonlinearity of sorption isotherm, the prediction uncertainty is higher. The pattern of the statistical moments of concentration is similar for cases with different correlation lengths of the parameters.

Citation: Chaudhuri, A., and M. Sekhar (2007), Stochastic finite element method for analysis of transport of nonlinearly sorbing solutes in three-dimensional heterogeneous porous media, *Water Resour. Res.*, *43*, W07442, doi:10.1029/2006WR004892.

1. Introduction

[2] The random spatial variability in the physical and chemical properties of the porous medium during the transport of reactive solutes in a heterogeneous porous medium result in (1) an uncertainty in the distribution of concentration field [*Tang and Pinder*, 1979; *Dagan*, 1989; *Kapoor and Gelhar*, 1994; *Chaudhuri and Sekhar*, 2005a] and (2) the field scale effective properties being quite different from the laboratory values [*Dagan*, 1989; *Gelhar*, 1993; *Hu et al.*, 1997; *Huang and Hu*, 2000; *Hassan*, 2001; *Chaudhuri and Sekhar*, 2005b]. Some of these studies have looked into the discrepancy between effective properties while modeling the system as heterogeneous medium instead of a homogeneous medium with uniform properties. Recently, *Lichtner and Tartakovsky* [2003] extended the investigations on the same aspect and studied the transient behavior of the theoretical effective reaction rate constant of a sorbing solute in a batch reactor system, with a heterogeneous grain and mineral distribution, and found that the behavior of the rate constant differs from that of a system with uniform properties. Another alternate approach pursued in the literature was to assess whether or not effective transport properties can be defined at all for some heterogeneous systems [*Guadagnini and Neuman*, 2001]. This aspect was addressed by the investigators for considering the format that a transport equation would take in order to be later solved consistently with the behavior of the system within the framework of random porous media.

[3] The solution of the stochastic partial differential equations (SPDE) governing the heterogeneous systems are often solved using either analytical methods or numerical methods [*de Marsily*, 1986]. When analytical methods [*Cushman*, 1997] are not suitable because of the complicated initial and boundary conditions, source/sink functions, nonuniform flow fields, and nonstationary properties, numerical methods are often used. The popular and simple Monte Carlo simulation method (MCSM) is based on generating a large number of equally likely random realizations for obtaining statistical moments of the dependent variable while using a solution of the deterministic system for each realization [*Bosma and van der Zee*, 1995; *Hassan et al.*, 1998]. This method is computationally exhaustive when a few thousands of realizations are required especially for a higher degree of medium heterogeneities along with a

[1]Department of Civil Engineering, Indian Institute of Science, Bangalore, India.

0043-1397/07/2006WR004892

higher space-time grid resolution. To avoid this difficulty associated with simulations involving multiple realizations, alternate methods such as moment equation method [*Guadagnini and Neuman*, 1999; *Guadagnini and Neuman*, 2001; *Wu et al.*, 2004; *Lu and Zhang*, 2004] and stochastic finite element method (SFEM) [*Spanos and Ghanem*, 1989] were proposed. These methods combine perturbation theory with numerical methods (for example, finite element, finite difference), which have been developed for solving the deterministic system. Some of these studies were aimed at comparing solutions obtained through these alternate approaches with that of the Monte Carlo simulations. The accuracy of these moment equation methods has been tested for consistency in the physical solution under transient cases for higher variances of random parameters. *Morales-Casique et al.* [2006] proposed an improved iterative moment equation method, which was found to provide good results for the nonreactive solute transport problem. It was shown that for some cases, the second-order solutions for the mean and the variance of concentration were inadequate to describe the physics involved in the transport process. Further, it was also shown that for higher variances of log hydraulic conductivity ($\sigma^2_{fK} > 0.3$), the comparison deteriorates. *Tartakovsky et al*. [2002] showed that in spite of using a higher order solution, the mean concentration showed oscillations and its convergence rate diminished with time even for small variances when analyzing a batch heterogeneous system in the absence of flow and diffusion processes.

[4] Stochastic finite element method, which is an alternate perturbation-based approach, was found to be a computationally attractive method for solving SPDEs. Recently, SFEM was applied in the groundwater literature for studying linear problems involving the flow and transport of solutes in three-dimensional heterogeneous porous medium [*Osnes and Langtangen*, 1998; *Ghanem*, 1998], and it was demonstrated that the method was computationally efficient in comparison with MCSM and was accurate even for a time-dependent linear transport problem for higher variances close to $\sigma^2_{fK} = 0.95$ [*Chaudhuri and Sekhar*, 2005b]. The formulation for applying SFEM to the nonlinear problems is not similar to that of the linear case as equations for lower order statistics involve the higher order statistics. The SFEM formulation for the nonlinear problems involves a different approach because of the type of the nonlinear terms in the transport equation. In addition, as the nonlinear problems would involve use of a suitable iterative scheme (for example, Newton-Raphson) within the time step of the numerical approach, it is required to assess the accuracy and computational efficiency of the SFEM developed for the nonlinear reactions, with respect to MCSM. *Lie and Qui* [2000] applied SFEM for the nonlinear structural engineering problems while analyzing nonlinear dynamics of a structure.

[5] Most of the reactive solutes follow a nonlinear reaction during the mass transfer process between aqueous and solid phase. Several studies have been made considering the coupled effects of nonlinear sorption and heterogeneity of medium properties. *Berglund and Cvetkovic* [1996] developed an analytical solution in Lagrangian framework for the displacement of purely advective and nonlinear sorbing solutes in a three-dimensional heterogeneous aquifer. Effect of the choice of isotherm equation representing nonlinear sorption on the cleanup time was studied. *Bosma et al.* [1996] modeled the average plume behavior in terms of the first two spatial moments using Monte Carlo simulations for physically and chemically heterogeneous porous media. Using a particle-tracking random walk technique, *Abulaban and Nieber* [2000] analyzed the transport of nonlinear sorbing solutes in two-dimensional steady and heterogeneous flow fields for various degrees of nonlinearity in the Freundlich isotherm equation, and behavior of the plume was quantified in terms of longitudinal spatial moments of various orders. In the above studies, the results were presented in terms of spatial moments of the plume. But for reliability analysis of concentration distribution, the mean and standard deviation of concentration are also quite important. *Xin and Zhang* [1998] developed an analytical solution of the mean and the standard deviation of concentration front for the one-dimensional transport of biodegrading solutes in a heterogeneous porous media. The problem setting uses simplified boundary conditions in order to apply an analytical approach. A spatial variation of the velocity due to random porosity field alone was considered in their study, while treating that hydraulic conductivity is not spatially varying random parameter. In the Lagrangian framework, *Severino et al.* [2000] derived the flux-averaged concentration of a nonlinearly sorbing solute, which was transported in a heterogeneous aquifer without considering the effects of pore-scale dispersion (pure advection case). Comparing the temporal plume moments obtained using stochastic analysis for a heterogeneous case with that of a deterministic equation, they presented the equivalent retardation coefficient and equivalent macrodispersivity at various spatial locations. It was observed that these increased with the travel distance. They also showed that the nonlinearity has a significant influence on the macrodispersivity and retardation.

[6] The objective of the present study is to develop a SFEM for the transport of the nonlinear sorbing solutes in a general three-dimensional heterogeneous porous media and test its performance. The motivation is that SFEM performed quite well for the linear transport problem, and relatively few attempts were made in the literature for using perturbation-based methods for the nonlinear problems while analyzing solute transport in a porous medium. In the proposed method, the nonlinear partial differential equation is transformed to a set of algebraic equations for each time step using the conventional finite element method (FEM). Later, a perturbation approximation is applied to the set of finite element equations. The SFEM formulation here uses a computationally efficient approach for computing the derivatives of concentration with respect to the random parameters [*Chaudhuri and Sekhar*, 2005a]. The accuracy and the computational efficiency of this method is compared with the commonly used MCSM by applying it on both one- and three-dimensional problems wherein the hydraulic conductivity, dispersivity, molecular diffusion coefficient, porosity, sorption coefficient, and first-order decay coefficient are assumed as random fields. Various cases are analyzed varying the coefficient of variation and correlation length of the random properties, while testing the computational efficiency. Results of spatial distribution

of statistical moments of concentration at large time are presented for the three-dimensional problem.

2. Problem Definition

[7] The governing equation for the transport of a nonlinearly sorbing and first-order decaying solute in a three-dimensional heterogeneous porous medium can be given as,

$$n(\mathbf{x})\frac{\partial c(\mathbf{x},t)}{\partial t}+\rho_b\frac{\partial s(\mathbf{x},t)}{\partial t} +\frac{\partial}{\partial x_i}\left(n(\mathbf{x})v_i(\mathbf{x})c(\mathbf{x},t)-n(\mathbf{x})D_{ij}(\mathbf{x})\frac{\partial c(\mathbf{x},t)}{\partial x_j}\right) +n(\mathbf{x})\gamma_d(\mathbf{x})c(\mathbf{x},t)+\rho_b\gamma_d(\mathbf{x})s(\mathbf{x},t)=0, \tag{1}$$

where $c(\mathbf{x}, t)$ and $s(\mathbf{x}, t)$ are concentration in the aqueous phase and sorbed phase, respectively, at location $\mathbf{x}$ and time t. The solute decay process in equation (1) is assumed that the solute decay occurs both in the aqueous and sorbed phases with the same rate. Also in equation (1), $n(\mathbf{x})$ and $\gamma_d(\mathbf{x})$ are the spatially varying porosity and decay coefficient, respectively. A nonlinear sorption isotherm is assumed to be valid here for describing the sorption process. In the literature, different isotherm equations are used to model the nonlinear sorption on the basis of the data obtained from the laboratory experiments. A general Langmuir-Freundlich isotherm discussed by *Berglund and Cvetkovic* [1996] that is applicable for various solutes is considered in this study. This nonlinear Langmuir-Freundlich isotherm is given by,

$$s(\mathbf{x},t)=k_d(\mathbf{x})g(c,\mathbf{x},t), \tag{2}$$

where ρ_b and $k_d(\mathbf{x})$ are bulk density of soil and sorption coefficient, respectively. Here the nonlinear reaction function $g(c, \mathbf{x}, t)$ is chosen as,

$$g(c,\mathbf{x},t)=\frac{(Bc(\mathbf{x},t))^m}{1+(Bc(\mathbf{x},t))^m} \tag{3}$$

The parameter B, which is used in the Langmuir-Freundlich isotherm, is called affinity parameter. In equation (1), $\mathbf{v}(\mathbf{x})$ is the pore water velocity vector, which is defined as $\mathbf{v}(\mathbf{x}) = \mathbf{q}(\mathbf{x}) / n(\mathbf{x})$. The seepage flux vector $\mathbf{q}(\mathbf{x})$ is obtained using the hydraulic conductivity tensor ($\mathbf{K}(\mathbf{x})$) and the hydraulic head ($H(\mathbf{x})$), on the basis of the Darcy equation as given by,

$$q_i(\mathbf{x})=-K_{ij}(\mathbf{x})\frac{\partial H(\mathbf{x})}{\partial x_j}. \tag{4}$$

Here $\mathbf{D}(\mathbf{x})$ is the hydrodynamic dispersion coefficient tensor, which is represented combining with the effective molecular diffusion coefficient in porous medium ($D_{\mathrm{m}}(\mathbf{x})$) and is given by,

$$D_{ij}(\mathbf{x})=\alpha(\mathbf{x})\left((1-\epsilon)\frac{v_i(\mathbf{x})v_j(\mathbf{x})}{v(\mathbf{x})}+\epsilon v(\mathbf{x})\delta_{ij}\right)+D_{\mathrm{m}}(\mathbf{x})\delta_{ij}. \tag{5}$$

In equation (5), $\alpha(\mathbf{x})$ is the longitudinal local dispersivity and ϵ is the ratio of transverse to longitudinal local dispersivity. In the above expression [equation (5)], δ_{ij} is Kronecker operator.

Equation (1) is solved for a set of initial and boundary conditions, which are written as,

$$\begin{aligned} &c(\mathbf{x},0)=c_0(\mathbf{x}),\ \text{for } \mathbf{x}\in\Omega,\\ &c(\mathbf{x},t)=c_b(\mathbf{x},t)\ \text{for } \mathbf{x}\in\Gamma_1,\\ &\text{and}\left(n(\mathbf{x})v_i(\mathbf{x})c(\mathbf{x},t)-n(\mathbf{x})D_{ij}(\mathbf{x})\frac{\partial c(\mathbf{x},t)}{\partial x_j}\right)n_{x_i}=f_b(\mathbf{x},t)\ \text{for } \mathbf{x}\in\Gamma_2. \end{aligned} \tag{6}$$

Here $c_0(\mathbf{x})$ is initial distribution of concentration while $c_b(\mathbf{x}, t)$ and $f_b(\mathbf{x}, t)$ are the time-dependent specified concentration and solute flux at the boundaries, respectively. Further, n_{x_i} is the direction cosine of the normal to the boundary surface along the x_i axis.

[8] The equation for the steady state flow in the domain with spatially varying hydraulic conductivity field is given by,

$$\frac{\partial}{\partial x_i}\left(K_{ij}(\mathbf{x})\frac{\partial H(\mathbf{x})}{\partial x_j}\right)=0. \tag{7}$$

Further, the specified boundary conditions governing the flow in the domain are given by,

$$\begin{aligned} &H(\mathbf{x})=H_b(\mathbf{x})\ \text{for } \mathbf{x}\in\Gamma_1^h\\ &\text{and } K_{ij}(\mathbf{x})\frac{\partial H(\mathbf{x})}{\partial x_j}n_{x_i}=q_b(\mathbf{x})\ \text{for } \mathbf{x}\in\Gamma_2^h. \end{aligned} \tag{8}$$

Equation (1) can be solved in the time domain by using the finite difference method. In the present study, the spatial part of equation (1) is solved using FEM. The Laplace domain FEM used in the SFEM [*Chaudhuri and Sekhar*, 2005a] is not suitable for the solution of the nonlinear reactive transport problem. The iterative approach involving the forward and inverse numerical Laplace transform cannot assure the convergence of the solution. Because of such difficulty, the SFEM in the time domain has to be derived. In the present study, the flow and solute transport equations are not coupled since the reactions do not alter the flow parameters (for example, hydraulic conductivity), and hence it is assumed that the flow remains unchanged. However, the flow and solute transport would be coupled and required to be solved simultaneously for a case such as hydraulic conductivity reduction occurring because of clogging or density-dependent fluid flow. Here, prior to solving equation (1), the velocity field is obtained by solving the governing flow equation (7).

3. Time Domain FEM Formulation for Nonlinearly Sorbing Solutes

[9] The governing nonlinear coupled partial differential equations (1), (2), and (3) can be solved using finite element method in a deterministic fashion, if the information pertaining to the spatially varying properties are available. The FEM approach for such a deterministic system is described below. For the sake of convenience in the finite element formulation, equation (2) is substituted in equation (1). For

any element (say pth), the finite element equation (FE) resulting from equation (1) is obtained as,

$$\int_{\Omega^e} n_p N_k(\mathbf{x}) N_l(\mathbf{x}) \mathrm{d}\mathbf{x} \frac{\mathrm{d}C_l(t)}{\mathrm{d}t} + \int_{\Omega^e} \rho_b k_{dp} N_k(\mathbf{x}) N_l(\mathbf{x}) \mathrm{d}\mathbf{x} \frac{\mathrm{d}G_l(t)}{\mathrm{d}t} + \int_{\Omega^e} \left(\frac{\partial N_k(\mathbf{x})}{\partial x_i} n_p \left(-v_{ip} N_l(\mathbf{x}) + D_{ij_p} \frac{\partial N_l(\mathbf{x})}{\partial x_j} \right) + n_p \gamma_{d_p} N_k(\mathbf{x}) N_l(\mathbf{x}) \right) \mathrm{d}\mathbf{x} C_l(t) + \int_{\Omega^e} \rho_b k_{dp} \gamma_{d_p} N_k(\mathbf{x}) N_l(\mathbf{x}) \mathrm{d}\mathbf{x} G_l(t) + \oint_{d\Omega^e} N_k(\mathbf{x}) \left(n_p v_{ip} N_l(\mathbf{x}) - n_p D_{ij_p} \frac{\partial N_l(\mathbf{x})}{\partial x_j} \right) n_{x_i} \mathrm{d}A C_l(t) = 0, \tag{9}$$

where $N_k(\mathbf{x})$ is the kth shape function, $C_k(t)$ and $G_k(t)$ are the concentration in aqueous phase and sorption component, respectively, at the kth node of any element. Equation (9) can be written as,

$$\Rightarrow [R_c]_p \{\dot{C}(t)\} + [R_g]_p \{\dot{G}(t)\} + [D_c]_p \{C(t)\} + [D_g]_p \{G(t)\} = \{C_b(t)\}_p. \tag{10}$$

Here the subscript 'p' corresponds to the property as well as the local matrix of pth element, and N is the number of elements used to discretize the domain. Assembling the local FE equations of each element, the global FE equation is obtained and expressed as,

$$[R_c]\{\dot{C}(t)\} + [R_g]\{\dot{G}(t)\} + [D_c]\{C(t)\} + [D_g]\{G(t)\} = \{C_b(t)\}. \tag{11}$$

Using the Crank-Nicholson formulation for the first-order time derivative, the global FE equation (11) can be further simplified as,

$$[D_1]\{C^{t+1}\} + [R_1]\{G^{t+1}\} = [D_2]\{C^t\} + [R_2]\{G^t\} + \theta\{C_b^{t+1}\} + (1-\theta)\{C_b^t\}, \tag{12}$$

where $[D_1] = \frac{1}{\Delta t}[R_c] + \theta[D_c]$, $[D_2] = \frac{1}{\Delta t}[R_c] - (1-\theta)[D_c]$, $[R_1] = \frac{1}{\Delta t}[R_g] + \theta[D_g]$, and $[R_2] = \frac{1}{\Delta t}[R_g] - (1-\theta)[D_g]$. Here Δt is the time interval. In the present study, θ is taken as 0.5 to obtain a second-order accurate solution in time. These global transport matrices ($[D_1]$, $[D_2]$, $[R_1]$, and $[R_2]$) as well as the source vectors ($\{C_b^t\}$, $\{C_b^{t+1}\}$) are obtained for the given boundary conditions of the solute concentration in aqueous phase. Isotherm equation (3) at each node and at each time step is expressed as,

$$G_i^{t+1} = \frac{\left(BC_i^{t+1}\right)^m}{1 + \left(BC_i^{t+1}\right)^m}. \tag{13}$$

The solution of the coupled nonlinear algebraic equations (12) and (13) can be solved by using either the Picard's iterative approach or the Newton-Raphson method.

4. SFEM Formulation for Nonlinearly Sorbing Solutes

[10] To use any numerical method of solution to a stochastic PDE, the random vectors of the uncertain governing parameters are formed by discretizing the random fields. In a perturbation-based SFEM, the random parameter of each element is decomposed into a mean part and a zero mean random part. From equations (9), (10), (11), and (12), it may be noted that the matrices derived in the previous section ($[D_1]$, $[D_2]$, $[R_1]$, and $[R_2]$) are functions of discretized random parameters. One can also note that the product of the two different random parameters is also appearing in the finite element formulation [equation (9)]. Similar to the discretized governing random parameters, these matrices are also decomposed into mean ($[\overline{D}_1]$, $[\overline{D}_2]$, $[\overline{R}_1]$, and $[\overline{R}_2]$) and zero mean random perturbed matrices ($[D_1]'$, $[D_2]'$, $[R_1]'$, and $[R_2]'$). The mean of the matrices is computed by taking the expectation over the expression. This results in these matrices ($[\overline{D}_1]$, $[\overline{D}_2]$, $[\overline{R}_1]$, and $[\overline{R}_2]$) being functions of individual random parameters as well as their product as given in equation (9). Under the approximation that the difference of the product of any two random variables and its ensemble average is negligible, the zero mean random perturbed part of the transport matrices ($[D_1]'$, $[D_2]'$, $[R_1]'$, and $[R_2]'$) becomes a linear functions of the random variables r'_p [*Chaudhuri and Sekhar*, 2005a]. Here the random components (r'_p, $p = 1, 2, \cdots, N_r$) correspond to the three components of velocity, local dispersivity, molecular diffusion, porosity, sorption coefficient, and decay coefficient of each element. N_r is the total number of random variables ($N_r = 8N$). The matrices $[D_1]$, $[D_2]$, $[R_1]$, and $[R_2]$ are expanded using the Taylor series about the mean value of the random parameters (r'_p, $p = 1, 2, \cdots, N_r$). Since the second and higher order derivatives of these matrices drop out being a linear case, the equations for the matrices can be further simplified and expressed as,

$$[D_1] = [\overline{D}_1] + [D_1]' = [\overline{D}_1] + \sum_{p=1}^{N_r} [D_1]_{r_p}^{(I)} r'_p \quad \text{and } [D_2] = [\overline{D}_2] + [D_2]' = [\overline{D}_2] + \sum_{p=1}^{N_r} [D_2]_{r_p}^{(I)} r'_p, \tag{14}$$

$$[R_1] = [\overline{R}_1] + [R_1]' = [\overline{R}_1] + \sum_{p=1}^{N_r} [R_1]_{r_p}^{(I)} r'_p \quad \text{and } [R_2] = [\overline{R}_2] + [R_2]' = [\overline{R}_2] + \sum_{p=1}^{N_r} [R_2]_{r_p}^{(I)} r'_p. \tag{15}$$

In the present formulation, $\Theta_{r_p}^{(I)} = \frac{\partial \Theta}{\partial r_p}$ and $\Theta_{r_p r_q}^{(II)} = \frac{\partial^2 \Theta}{\partial r_p \partial r_q}$, where Θ may be any scalar, vector, or matrix. The output variables, i.e., the concentration of the aqueous and the sorbed phases, are unknown nonlinear functions of the random system parameters (r'_p, $p = 1, 2, \cdots, N_r$). These output variables are expanded in the Taylor series as shown below,

$$\{C^{t+1}\} = \{C^{t+1}\}^{(0)} + \sum_{p=1}^{N_r} \{C^{t+1}\}_{r_p}^{(I)} r'_p + \frac{1}{2} \sum_{p=1}^{N_r} \sum_{q=1}^{N_r} \{C^{t+1}\}_{r_p r_q}^{(II)} r'_p r'_q \cdots, \tag{16}$$

$$\{G^{t+1}\} = \{G^{t+1}\}^{(0)} + \sum_{p=1}^{N_r} \{G^{t+1}\}_{r_p}^{(I)} r'_p + \frac{1}{2} \sum_{p=1}^{N_r} \sum_{q=1}^{N_r} \{G^{t+1}\}_{r_p r_q}^{(II)} r'_p r'_q \cdots. \tag{17}$$

In the present study, derivatives higher than second-order derivatives in the Taylor series expansion of concentrations are neglected. By taking the expectation of equation (16), the mean of the aqueous concentration is obtained and expressed as,

$$\left\{\overline{C}^{t+1}\right\} = \left\{C^{t+1}\right\}^{(0)} + \frac{1}{2}\sum_{p=1}^{N_r}\sum_{q=1}^{N_r}\left\{C^{t+1}\right\}^{(II)}_{r_p r_q}\overline{r'_p r'_q}. \tag{18}$$

Since the expression of mean of concentration includes the second-order derivatives and the covariance of the random parameters, the present study provides the second-order accurate mean concentration [*Kleiber and Hien*, 1992]. The equation for the random perturbed component of aqueous concentration ($\{C^{t+1}\}'$) is obtained by subtracting equation (18) from equation (16) and approximating $r'_p r'_q - \overline{r'_p r'_q}$ as negligible, resulting in the expression,

$$\left\{C^{t+1}\right\}' = \sum_{p=1}^{N_r}\left\{C^{t+1}\right\}^{(I)}_{r_p} r'_p. \tag{19}$$

Since ($\{C^{t+1}\}'$) contains only first-order derivatives, the first-order accurate covariance matrix of the aqueous concentration at any two different times instances (t_1 and t_2) is written as,

$$[\mathrm{CV}]_{cc} = \sum_{p=1}^{N_r}\sum_{q=1}^{N_r}\left\{C^{t_1}\right\}^{(I)}_{r_p}\left\{C^{t_2}\right\}^{(I)T}_{r_q}\overline{r'_p r'_q}. \tag{20}$$

In a similar way, the mean and the covariance matrix for the sorbed phase component ($\{G^{t+1}\}$) can also be expressed.

[11] In the next part of this section, the derivatives of $\{C^{t+1}\}$ and $\{G^{t+1}\}$ are derived by substituting equations (14), (15), (16), and (17) into equations (12) and (13). Putting $r'_p = 0$ for $p = 1, 2, \cdots, N_r$ into equations (12) and (13), the zeroth-order derivatives ($\{C^{t+1}\}^{(0)}$ and $\{G^{t+1}\}^{(0)}$) are obtained and expressed as,

$$\begin{aligned}\left[\overline{D}_1\right]\left\{C^{t+1}\right\}^{(0)} + \left[\overline{R}_1\right]\left\{G^{t+1}\right\}^{(0)} &= \left[\overline{D}_2\right]\left\{C^{t}\right\}^{(0)} \\ &+ \left[\overline{R}_2\right]\left\{G^{t}\right\}^{(0)} + \theta\left\{C_b^{t+1}\right\} + (1-\theta)\left\{C_b^{t}\right\}\end{aligned} \tag{21}$$

$$G_i^{t+1,(0)} = \frac{\left(BC_i^{t+1,(0)}\right)^m}{1+\left(BC_i^{t+1,(0)}\right)^m}. \tag{22}$$

To compute the zeroth-order derivatives, the coupled nonlinear algebraic equations (21) and (22) have to be solved. The solution of these nonlinear equations can be performed by the Picard's iteration approach. But this approach may generate a periodic solution in some cases instead of the fixed-point solution for the nonlinear dynamical systems [*Strogatz*, 1994]. Hence, in the present study, the Newton-Raphson method is adopted. To solve by the Newton-Raphson method, a new vector ($\{E^{t+1}\}$) for equation (21) is defined as,

$$\begin{aligned}\left\{E^{t+1}\right\} = \left[\overline{D}_1\right]\left\{C^{t+1}\right\}^{(0)} + \left[\overline{R}_1\right]\left\{G^{t+1}\right\}^{(0)} - \left[\overline{D}_2\right]\left\{C^{t}\right\}^{(0)} \\ - \left[\overline{R}_2\right]\left\{G^{t}\right\}^{(0)} - \theta\left\{C_b^{t+1}\right\} - (1-\theta)\left\{C_b^{t}\right\}.\end{aligned} \tag{23}$$

In a more explicit way, this equation with ith index can be rewritten as,

$$\begin{aligned}E_i^{t+1} = \sum_{j=1}^{M}\left(\overline{D}_{1ij}C_j^{t+1,(0)} + \overline{R}_{1ij}G_j^{t+1,(0)} - \overline{D}_{2ij}C_j^{t,(0)} - \overline{R}_{2ij}G_j^{t,(0)}\right) \\ - \theta C_{b_i}^{t+1} - (1-\theta)C_{b_i}^{t},\end{aligned} \tag{24}$$

where M is the number of nodes with unknown concentration. This vector, $\{E^{t+1}\}$, converges to zero when solution converges to the exact solution. The ijth element of the Jacobian matrix $[\Delta E^{t+1}]$, which is obtained from equation (24) using the expression in equation (22), is expressed as,

$$\begin{aligned}\Delta E_{ij}^{t+1} &= \frac{\partial E_i^{t+1}}{\partial C_j^{t+1,(0)}} = \overline{D}_{1ij} + \overline{R}_{1ij}\frac{\partial G_j^{t+1,(0)}}{\partial C_j^{t+1,(0)}} \\ &= \overline{D}_{1ij} + \overline{R}_{1ij}\frac{mB^m\left(C_j^{t+1,(0)}\right)^{m-1}}{\left(1+\left(BC_j^{t+1,(0)}\right)^m\right)^2}.\end{aligned} \tag{25}$$

In a more compact form, equation (25) can be rewritten as,

$$\left[\Delta E^{t+1}\right] = \left[\overline{D}_1\right] + \left[\overline{R}_1\right]\left[\Delta R^{t+1}\right], \tag{26}$$

where $[\Delta R^{t+1}]$ is a diagonal matrix and its jth diagonal is $\frac{\partial G_j^{t+1,(0)}}{\partial C_j^{t+1,(0)}}$. The solution at kth iteration is expressed as,

$${}^{k}\left\{C^{t+1}\right\}^{(0)} = {}^{k-1}\left\{C^{t+1}\right\}^{(0)} - \left[{}^{k-1}\left[\Delta E^{t+1}\right]\right]^{-1}{}^{k-1}\left\{E^{t+1}\right\}. \tag{27}$$

Here ${}^{k}\{C^{t+1}\}^{(0)}$ indicates the value of $\{C^{t+1}\}^{(0)}$ at kth iteration. In this iterative method, the initial guess of the solution (concentration at any time step) is taken as the average value of the concentration obtained in the previous time step of the nonlinear problem and that of the linear sorption problem for the current time step. For the first time step, however, the linear sorption problem is used as the initial guess concentration. The convergence criteria is used as,

$$\left(\sum_{i=1}^{N}\left(\frac{{}^{k}C_i^{t+1,(0)} - {}^{k-1}C_i^{t+1,(0)}}{{}^{k-1}C_i^{t+1,(0)}}\right)^2\right)^{\frac{1}{2}} \le 0.0001. \tag{28}$$

The equations for the first-order derivative of concentration and sorption component with respect to any random variable r_p are obtained by equating the coefficients of random variable (r'_p) in both sides of equations (12) and (13), respectively. These equations are expressed as,

$$[D_1]^{(I)}_{r_p}\{C^{t+1}\}^{(0)}+[\overline{D}_1]\{C^{t+1}\}^{(I)}_{r_p}+[R_1]^{(I)}_{r_p}\{G^{t+1}\}^{(0)}+[\overline{R}_1]\{G^{t+1}\}^{(I)}_{r_p} = \left([D_2]^{(I)}_{r_p}\{C^{t}\}^{(0)}+[\overline{D}_2]\{C^{t}\}^{(I)}_{r_p}+[R_2]^{(I)}_{r_p}\{G^{t}\}^{(0)}+[\overline{R}_2]\{G^{t}\}^{(I)}_{r_p}\right), \tag{29}$$

$$G^{t+1,(I)}_{i,r_p}=\frac{\partial G^{t+1,(0)}_j}{\partial C^{t+1,(0)}_j}C^{t+1,(I)}_{i,r_p}=\frac{mB^m\left(C^{t+1,(0)}_i\right)^{m-1}}{\left(1+\left(BC^{t+1,(0)}_i\right)^m\right)^2}C^{t+1,(I)}_{i,r_p}. \tag{30}$$

It is noted that equations (29) and (30) for the first-order derivatives of the concentration and sorption component are a coupled system of linear algebraic equations. Using equations (26) and (30), the terms in equation (29), $[\overline{D}_1]\{C^{t+1}\}^{(I)}_{r_p}+[\overline{R}_1]\{G^{t+1}\}^{(I)}_{r_p}$, can be replaced by $[\Delta E^{t+1}]\{C^{t+1}\}^{(I)}_{r_p}$ to obtain $\{C^{t+1}\}^{(I)}_{r_p}$ and is given as,

$$\begin{aligned}\{C^{t+1}\}^{(I)}_{r_p}=[\Delta E^{t+1}]^{-1}\Big(&-[D_1]^{(I)}_{r_p}\{C^{t+1}\}^{(0)}-[R_1]^{(I)}_{r_p}\{G^{t+1}\}^{(0)}\\&+[D_2]^{(I)}_{r_p}\{C^{t}\}^{(0)}+[\overline{D}_2]\{C^{t}\}^{(I)}_{r_p}\\&+[R_2]^{(I)}_{r_p}\{G^{t}\}^{(0)}+[\overline{R}_2]\{G^{t}\}^{(I)}_{r_p}\Big).\end{aligned} \tag{31}$$

Using equation (30) along with equation (31), the expression for the sorption component $\{G^{t+1}\}^{(I)}_{r_p}$ can be obtained. Similar to the first-order derivative, the equations for the second-order derivative of aqueous concentration ($\{C^{t+1}\}^{(II)}_{r_pr_q}$) is also obtained by equating the coefficients of $r'_pr'_q$ in equation (12) after substituting equations (14), (15), (16), and (17). In terms of the first-order derivatives of the current and previous time steps as well as second-order derivatives at previous time step, the equation for second-order derivatives of the concentration is written as,

$$\begin{aligned}&[D_1]^{(I)}_{r_p}\{C^{t+1}\}^{(I)}_{r_q}+[D_1]^{(I)}_{r_q}\{C^{t+1}\}^{(I)}_{r_p}+[\overline{D}_1]\{C^{t+1}\}^{(II)}_{r_pr_q}\\&\quad+[R_1]^{(I)}_{r_p}\{G^{t+1}\}^{(I)}_{r_q}+[R_1]^{(I)}_{r_q}\{G^{t+1}\}^{(I)}_{r_p}+[\overline{R}_1]\{G^{t+1}\}^{(II)}_{r_pr_q}\\&=[D_2]^{(I)}_{r_p}\{C^{t}\}^{(I)}_{r_q}+[D_2]^{(I)}_{r_q}\{C^{t}\}^{(I)}_{r_p}+[\overline{D}_2]\{C^{t}\}^{(II)}_{r_pr_q}\\&\quad+[R_2]^{(I)}_{r_p}\{G^{t}\}^{(I)}_{r_q}+[R_2]^{(I)}_{r_q}\{G^{t}\}^{(I)}_{r_p}+[\overline{R}_2]\{G^{t}\}^{(II)}_{r_pr_q},\end{aligned} \tag{32}$$

Because of the expansion of the matrices ($[D_1]$, $[D_2]$, $[R_1]$, and $[R_2]$) up to first-order terms, in equations (14) and (15), the second-order derivatives of these matrices are not appearing in equation (32). From equation (17), the second-order derivative ($\{C^{t+1}\}^{(II)}_{r_pr_q}$) can be directly obtained and given by,

$$\begin{aligned}G^{t+1,(II)}_{i,r_pr_q}=&\frac{mB^m\left(C^{t+1,(0)}_i\right)^{m-1}}{\left(1+\left(BC^{t+1,(0)}_i\right)^m\right)^2}C^{t+1,(II)}_{i,r_pr_q}\\&+\frac{mB^m\left(C^{t+1,(0)}_i\right)^{m-1}\left(m-1-(m+1)\left(BC^{t+1,(0)}_i\right)^m\right)}{\left(1+\left(BC^{t+1,(0)}_i\right)^m\right)^3}\\&\times C^{t+1,(I)}_{i,r_p}C^{t+1,(I)}_{i,r_q}=\frac{mB^m\left(C^{t+1,(0)}_i\right)^{m-1}}{\left(1+\left(BC^{t+1,(0)}_i\right)^m\right)^2}C^{t+1,(II)}_{i,r_pr_q}+G_{1i}.\end{aligned} \tag{33}$$

Here the term G_{1i} is computed from the known first-order derivatives. Equations (32) and (33) are a system of coupled linear equations, and substituting the expression of $G^{t+1,(II)}_{i,r_pr_q}$ [equation (33)] in equation (32), the second-order derivative of the aqueous concentration with respect to r_p and r_q are given as,

$$\begin{aligned}\{C^{t+1}\}^{(II)}_{r_pr_q}=[\Delta E^{t+1}]^{-1}\Big(&-[D_1]^{(I)}_{r_p}\{C^{t+1}\}^{(I)}_{r_q}-[D_1]^{(I)}_{r_q}\{C^{t+1}\}^{(I)}_{r_p}\\&-[R_1]^{(I)}_{r_p}\{G^{t+1}\}^{(I)}_{r_q}-[R_1]^{(I)}_{r_q}\{G^{t+1}\}^{(I)}_{r_p}-[\overline{R}_1]\{G_1\}\\&+[D_2]^{(I)}_{r_p}\{C^{t}\}^{(I)}_{r_q}+[D_2]^{(I)}_{r_q}\{C^{t}\}^{(I)}_{r_p}+[\overline{D}_2]\{C^{t}\}^{(II)}_{r_pr_q}\\&+[R_2]^{(I)}_{r_p}\{G^{t}\}^{(I)}_{r_q}+[R_2]^{(I)}_{r_q}\{G^{t}\}^{(I)}_{r_p}+[\overline{R}_2]\{G^{t}\}^{(II)}_{r_pr_q}\Big).\end{aligned} \tag{34}$$

When the expectation of the third term in equation (17) is taken, the second term of equation (33) for $G^{t+1,(II)}_{i,r_pr_q}$ results in an additional term involving the variance of G^{t+1}_i. Thus the mean of concentration becomes a function of variance of concentration for nonlinear sorption problem.

[12] The proposed SFEM does not require the solution of the linear equation for each second-order derivative of the concentration ($\{C^{t+1}\}^{(II)}_{rprq}$). The double summation (i.e., second-order term) in equation (18) is calculated directly. During computation of the double summation, the terms like $\sum_{q=1}^{N_r}\{C^{t+1}\}^{(I)}_{r_q}\overline{r'_pr'_q}$ is calculated by matrix multiplication of covariance matrix of the parameters and matrix composed of the first-order derivative of the concentration. Later premultiplication by matrix $[D_1]^{(I)}_{r_p}$ with the above expression is performed by taking advantage of the sparse nature of $[D_1]^{(I)}_{r_p}$. This approach is carried out for all value of the index p and other terms in equation (34). The efficient algorithm used for the matrix multiplication was discussed in the work of *Chaudhuri and Sekhar* [2005a].

[13] In equations (18) and (20), the mean aqueous concentration and covariance of aqueous concentration are expressed in terms of the covariances of the element random properties. The covariance matrix of the random properties (which are piecewise linear inside an element) is derived from the given variances and spatial correlation functions for the random fields. In section 5, a brief description of the random properties and the procedure to obtain the

covariance matrix are provided. For solving the transport problem, the mean and the covariance of velocity vectors and the dispersion coefficient tensors are required to be derived, which are obtained from the mean and the covariance of the hydraulic conductivity and the local scale dispersivity. The equations and the procedure for obtaining these stochastic quantities of velocity and dispersion coefficient are also separately given in Appendix A.

5. Descriptions of the Random Fields

[14] The computational cost of SFEM increases linearly with the increase in the number of random parameters since higher number of sensitivity equations have to be solved with the increase in the random parameters. On the other hand, the convergence rate of MCSM for a specified number of realizations does not depend on the number of random parameters. The modeling of multiple parameters as a random function can also affect the accuracy of SFEM when few of the random parameters appear as a product in the governing equation. In this study, as for example, the transport equation (1) consists of the product of porosity and decay coefficient. The effect of perfect correlation among parameters is inferior to the case with no correlation. In the present study, in order to test the efficiency and accuracy of the SFEM, multiple random parameters are considered. The hydraulic conductivity is commonly assumed to follow a lognormal distribution [*Gelhar*, 1993; *Cushman*, 1997]. Porosity is either modeled as a normal [*Xin and Zhang*, 1998] or a lognormal [*Hassan*, 2001] random spatial function. The correlation between porosity and hydraulic conductivity depends on the type of the aquifer materials [*Doyen*, 1988; *Gelhar et al.*, 1992; *Hassan et al.*, 1998]. Any functional relation between them provides perfect correlation. In the case of no correlation between hydraulic conductivity and porosity, the correlation length of the two need not be same [*Hassan*, 2001]. Similarly, the sorption coefficient is also modeled either as a normal or a lognormal distribution in the literature [*Roberts et al.*, 1986; *Hu et al.*, 1997; *Rajaram*, 1997; *Wu et al.*, 2004; *Fernandez-Garcia et al.*, 2005]. When sorption processes are completely linked to grain surface areas, *Garabedian et al.* [1988] showed that hydraulic conductivity has perfect negative correlation with the sorption affinity parameter. When the correlation coefficient is negative, it was observed that the mixing of the reactive solute transport is enhanced [*Valocchi*, 1989]. But *Robin et al.* [1991] showed that the correlation between log hydraulic conductivity and sorption coefficient depends on the scale and direction because of the variation of mineralogical, chemical, and physical characteristics of the aquifer. For analyzing the solute transport problem in a radial flow field using Monte Carlo simulation, *Castillo-Cerda et al.* [2004] considered an imperfect correlation between the sorption coefficient and the hydraulic conductivity, which allowed choosing various variogram models with different parameters. From the experiments of strontium transport in the Borden aquifer, it was observed that the correlation length of the sorption coefficient is smaller than that of the hydraulic conductivity along horizontal direction but the opposite along vertical direction. Using facies-based approach, *Allen-King et al.* [1998] showed that the correlation between these two parameters is not the same for different facies. An empirical relationship between the local dispersivity and the grain size distribution was given by *Harleman* [1963], which suggests a positive correlation between the local dispersivity and the hydraulic conductivity. On the contrary, *Perfect et al.* [2002] showed that the local dispersivity increased sequentially moving from the coarser to finer textural classes. Since the studies pertaining to this relationship are few, in this study, a perfect correlation between them is used as a working assumption. Decay rate can also be modeled as a lognormal random field [*Miralles-Wilhelm and Gelhar*, 2000; *Metzger et al.*, 1999]. In the literature [*Bodin et al.*, 2003; *Ohlsson and Neretnieks*, 1995], the effective molecular diffusion coefficient was shown as a function of molecular diffusion coefficient of the solute in free water and the formation factor. The formation factor in turn is related to the porosity through a power law relationship from experimental investigations [*Sato*, 1999; *Boving and Grathwohl*, 2001]. Since porosity varies spatially, the effective molecular diffusion can also be considered as a spatially varying random field. Diffusion coefficient was considered to follow either a uniform or a lognormal distribution by *Haggerty and Gorelick* [1995]. On the basis of these earlier works, in the present study, all the flow and transport properties, which are considered as random fields, are assumed to follow a lognormal distribution. However, this assumption is not a limitation for the proposed SFEM. The random fields are assumed as statistically homogeneous and described by a Gaussian (squared exponential) type correlation function. When the parameters are perfectly either positively or negatively correlated they follow the same correlation function and the correlation length [*Hu et al.*, 1997; *Ghanem*, 1998; *Wu et al.*, 2004]. In the literature, it is a common practice to use the same correlation function and the same correlation length for various random parameters during the testing of performance of any numerical method. However, it may be noted that for specific applications experimentally derived correlations functions, if available, can also be used in the SFEM. The correlation coefficient between the values of the parameters at any two locations is given by, $\rho(\mathbf{x}) = \exp(-(\frac{x_1}{\lambda_1})^2 - (\frac{x_2}{\lambda_2})^2 - (\frac{x_3}{\lambda_3})^2)$. The covariance matrix for the random element properties is determined from the correlation function and their variances using the local averaging method [*Vanmarcke*, 1983]. Using this method, the correlation coefficient of the logarithm of the parameters (f_p and f_q) is expressed as,

$$\rho_{f_p f_q} = \frac{1}{V_p V_q} \int_{V_p} \int_{V_q} \rho(\mathbf{x}_p - \mathbf{x}_q) \mathrm{d}\mathbf{x}_p \mathrm{d}\mathbf{x}_q. \tag{35}$$

Further, the correlation coefficient between any two random parameters can be determined from the correlation coefficient between them. For example, between K_p and k_{d_q} this can be given as,

$$\rho_{K_p k_{d_q}} = \frac{K_G k_{dG}}{\sigma_K \sigma_{k_d}} \exp\left(\frac{1}{2}\left(\sigma_{f_K}^2 + \sigma_{f_{k_d}}^2\right)\right)\left(\exp\left(\rho_{f_{K_p} f_{k_{d_q}}} \sigma_{f_K} \sigma_{f_{k_d}}\right) - 1\right), \tag{36}$$

where f_{K_p} and $f_{k_{dq}}$ are log of K_p and k_{d_q}, respectively. This expression is derived theoretically without using any physical basis. If the expressions based on physical experiments are available, they can be directly incorporated in the SFEM. In a similar fashion, the correlation coefficient between any other two random parameters can also be

obtained. In special cases, when the values of the random parameters are known at a few locations, the variance should be zero at those locations. In such circumstances, the corresponding elements of the derived covariance matrix conditioned to measurements should vanish. Since the proposed SFEM uses directly the covariance matrix of the random parameters, such a conditioned covariance matrix can be used as an input to the SFEM.

6. Results and Discussion

[15] The SFEM developed in section (4) is applied for studying the probabilistic analysis of the transport of an equilibrium nonlinear sorbing solute in a heterogeneous porous media. Both one- and three-dimensional problems are analyzed for a set of parameters to study the effect on the probabilistic behavior of solute concentration. The accuracy of the SFEM is verified by comparing with the MCSM for both the one- and three-dimensional problems. The comparison between the methods is made while considering a set of coefficient of variation (COV) of the random parameters.

6.1. One-Dimensional Problem

[16] The transport of equilibrium nonlinear sorbing solute in a one-dimensional column is analyzed in this subsection. A uniform specific discharge occurs in the one-dimensional column even in the presence of spatially varying random hydraulic conductivity. Theoretically, the velocity of flow behaves as a random variable and its variance approaches to zero as the length of the one-dimensional column approaches infinity. For each realization of hydraulic conductivity in the one-dimensional column, the velocity of flow is constant and is given by the product of the piezometric head gradient and conductivity harmonic mean. In a finite domain, the harmonic mean depends on the variation of hydraulic conductivity values. The scale of variation of hydraulic conductivity further depends on the ratio of length of the column and correlation length. The harmonic mean of hydraulic conductivity may vary between any two realizations. However, a finite variance in velocity is obtained when using MCSM combined with a numerical method for a column of finite length.

[17] Hence, in order to use a consistent solution of the stochastic flow problem in the transport problem, the hydraulic conductivity is assumed as a deterministic variable for cases 1A to 1D (Table 1) while treating porosity, local scale dispersivity, diffusion coefficient, and sorption coefficient as spatially varying random functions. Further, simulations are also made considering hydraulic conductivity as a random parameter as well, which corresponds to cases 1E and 1F. In all these cases, the random parameters except the sorption coefficient are considered to be positively correlated, while the random sorption coefficient is assumed to have negative correlation with the rest of the other random parameters. However, there exists experimental evidences that in the case of solute undergoing linear reversible instantaneous equilibrium in a saturated medium, the sorption coefficient can be either positively or negatively correlated with hydraulic conductivity. Since negative correlation gives a higher uncertainty, this correlation behavior is used here in all the cases. Further in this study, it is assumed that all the random variables have the same covariance function. The spatial correlation function and the correlation length for each of the random fields are chosen same for testing the SFEM rather than looking into their field characteristics as discussed in section 5. However, it may be noted that the SFEM proposed as such can take any specified correlation function and correlation length for a random field. For numerical simulation, all variables are made dimensionless with respect to the height of the column (h) and pore water velocity (v). The dimensionless concentration of the pollutant at dimensionless depth ($x_3 = \tilde{x}_3 / h$) and dimensionless time ($t = v\tilde{t} / h$) is defined as $c(x_3, t) = \tilde{c}(\tilde{x}_3, \tilde{t})/c_0$. Further, $\alpha = \tilde{\alpha} / h$, $D_m(x_3) = \tilde{D}(\tilde{x}_3) / (vh)$, and $\gamma_d(x_3) = \tilde{\gamma}_d(\tilde{x}_3)h / v$ are the dimensionless local scale dispersivity, diffusion coefficient, and the decay coefficient, respectively. Here ~ corresponds to the dimensional quantity. The one-dimensional problem has been analyzed using the following values of the properties, $\overline{n} = 0.4$, $\overline{\gamma}_d = 0.005$, $\overline{k}_d\rho_b = 0.2$, $\overline{\alpha} = 0.01$, $\overline{D}_m = 0.01$, $m = 0.8$, and $B = 67.9$. For the one-dimensional random field, the correlation length λ is chosen as 0.02 (cases 1A–1D). For these cases, the ratio of the length of the column to the correlation length is 50. The domain is discretized into 150 elements for a unit dimensionless length. The transport problem is dispersion dominated and the numerical grid Peclet number is close to 0.5. The accuracy and efficiency of SFEM is compared with the Monte Carlo simulation method (with 2000 realizations) using results obtained for various cases, which pertain to various values of coefficient of variation of random parameters as listed in Table 2. The comparison of the mean and the standard deviation of the concentration obtained by SFEM and MCSM is shown in Figures 1b, 1c, 2b, 2c, 3b, 3c, 4b, 4c, 5b, 5c, 6b, and 6c for the six cases (cases 1A–1F). Many experimental investigations, which were reported in the literature, show that the COV of the pore scale parameters (such as porosity, sorption coefficient, decay coefficients, etc.) do not vary much. The maximum value of the COV of the pore scale parameters, which is considered in case 1D is 1.0 (which corresponds to a $\sigma_{f_n} = 0.83$). The plots are presented in terms of the dimensionless mean and standard deviation of concentration along the length of the column at various time steps. The mean concentration breakthrough curves at various time steps computed using SFEM are found to have sharp fronts, and their spread does not increase with time as expected for the case of a nonlinear sorption problem. On the other hand, in general, the results obtained using MCSM show that the mean concentration follows a dispersive front behavior which increases with time. This pattern gets amplified for a higher coefficient of variation of system parameters as shown in Figures 1b, 2b, 3b, and 4b. It is

Table 1. Coefficients of Variation of Random Properties for Various Cases

	$\{n, k_d, \alpha, D_m, \gamma_d\}$		K	
Case	COV	λ	COV	λ
1A	0.30	0.02	–	–
1B	0.50	0.02	–	–
1C	0.75	0.02	–	–
1D	1.00	0.02	–	–
1E	0.50	0.02	0.50	0.02
1F	0.50	0.02	0.50	0.20

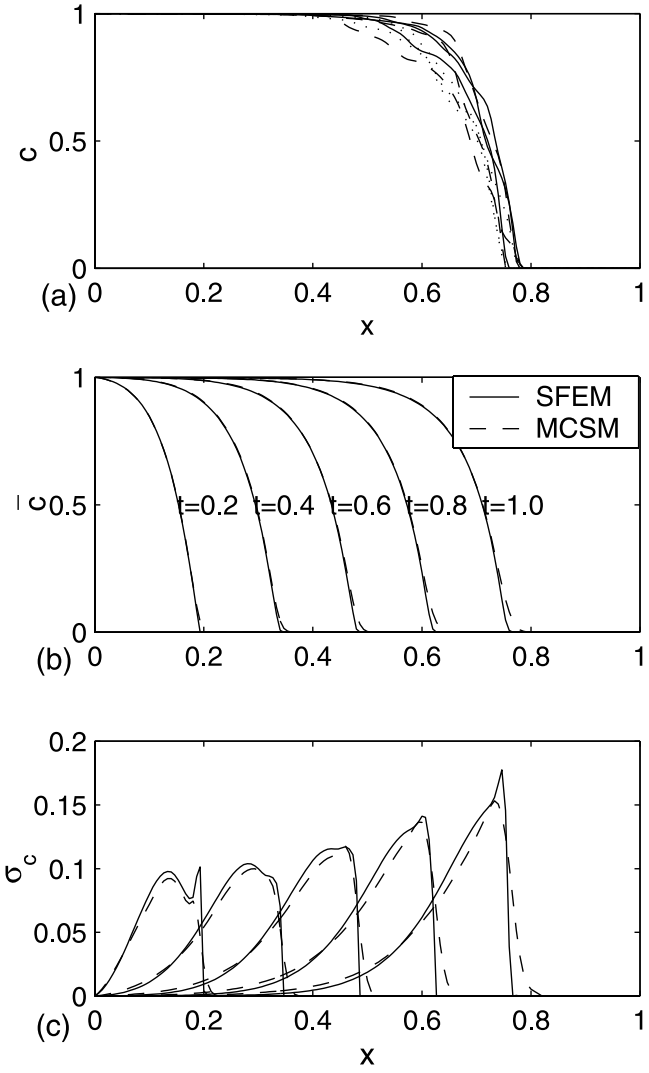

Figure 1. Concentration plot for case 1A. (a) Realizations generated using MCSM for time $t = 1.0$, (b) comparison of mean concentration between SFEM and MCSM at different time, and (c) comparison standard deviation of concentration between SFEM and MCSM.

also observed that the deviation between mean concentration obtained using SFEM and MCSM increases with time near the end of the front location. However, in the rest of the locations, the mean concentration is computed accurately using SFEM. It may be noted here that mean concentration is computed in SFEM with second-order accuracy. The standard deviations of concentration in all of the cases are observed to be the highest at the concentration front location. Further, the peak of the standard deviation obtained by MCSM is lower and shows a longer tail in comparison to that obtained by SFEM. The results of standard deviation of concentration obtained using SFEM compares well with that of MCSM much better prior to the front location, which suggests that SFEM is able to compute the steady state values of the standard deviation accurately.

[18] The additional effect of uncertainty due to random variation of hydraulic conductivity can be observed from Figure 5 for case 1E, which uses the same correlation length as used for cases 1A–1D. When the hydraulic conductivity is a random parameter, for the reasons discussed earlier, the flow problem dimension used is four times higher than the transport problem in order to have a better representation of the flow field in the transport problem for various realizations of MCSM and to be consistent, the same is adopted for SFEM as well. Hence the ratio of the length of the column to the correlation length used for case 1E is 200. Figure 5a shows the spreading of the concentration front for different realizations increases because of the variation in the flow velocity influenced mainly by the hydraulic conductivity in spite of using a larger domain. A comparison of case 1E with case 1B (equivalent case in all aspects except variance in hydraulic conductivity) indicates that the mean concentration fronts (Figure 5b) for case 1E have a lesser spread for SFEM simulations. The prediction uncertainty of the concentration is relatively higher for case 1E with respect to case 1B for the SFEM simulations. The MCSM results, on the other hand, give comparatively similar values between the two cases. In order to test the effects of hydraulic

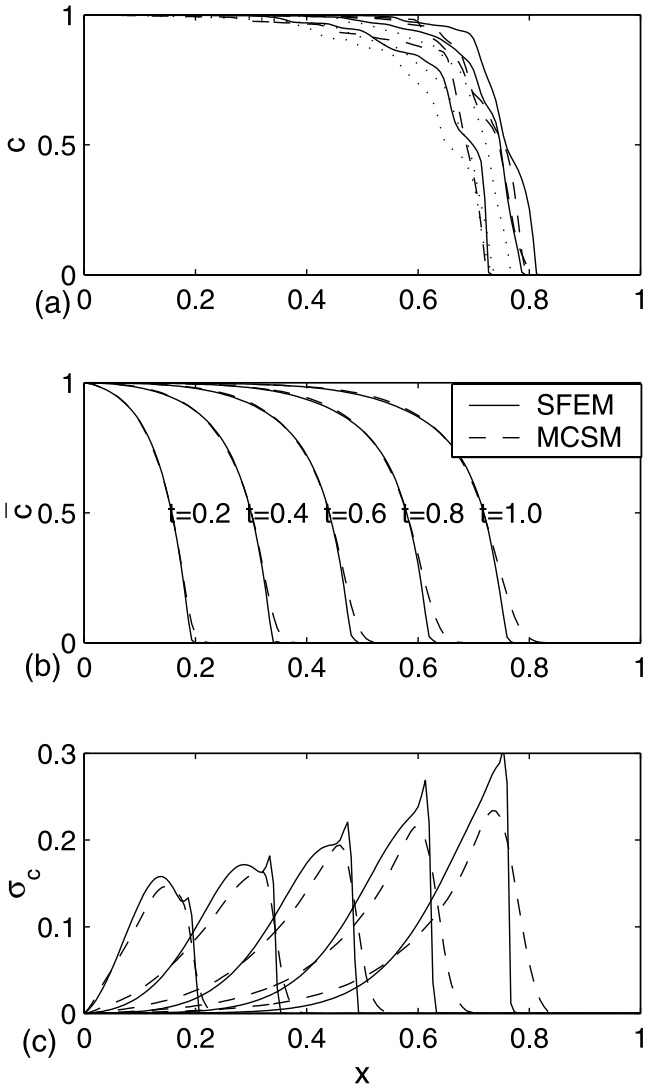

Figure 2. Concentration plot for case 1B. (a) Realizations generated using MCSM for time $t = 1.0$, (b) comparison of mean concentration between SFEM and MCSM at different time, and (c) comparison standard deviation of concentration between SFEM and MCSM.

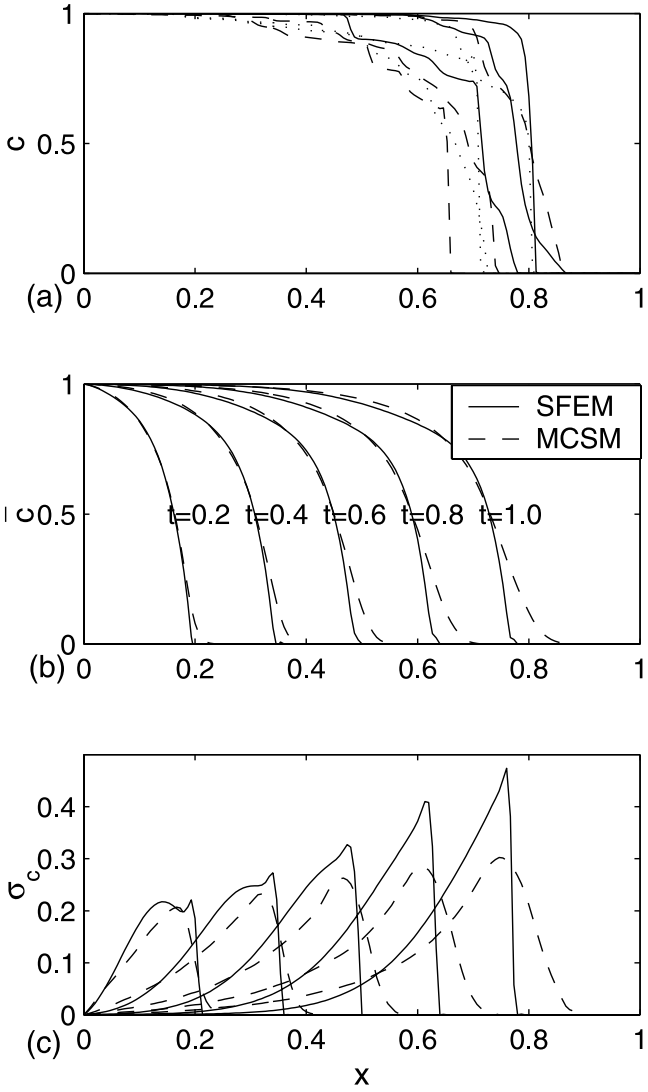

Figure 3. Concentration plot for case 1C. (a) Realizations generated using MCSM for time $t = 1.0$, (b) comparison of mean concentration between SFEM and MCSM at different time, and (c) comparison standard deviation of concentration between SFEM and MCSM.

conductivity further, simulations are made with case 1F, which uses the same variances of all parameters as in case 1E while the correlation length of the hydraulic conductivity being one order higher than case 1E. Here the ratio of the length of the column to the correlation length reduces to 20. The comparison with MCSM, shows that the results further deteriorate for the case 1F (Figure 6), relative to cases 1E and 1B. In this case, the uncertainty obtained by both SFEM and MCSM are higher than that of case 1E but SFEM produces significantly higher values. In the case 1F, the variation of flow velocity is higher than that of case 1E. This can be observed by comparing the travel distance of the solute plume in the Figure 6a. Since the velocity which is the input for the transport problem has a higher variation, the prediction uncertainty of concentration is high and the performance of SFEM is poor. For cases 1E and 1F, the results indicate that the mean front is moving at a lower velocity than that of cases 1A–1D. This is due to a lower effective flow velocity resulting from the randomness in the hydraulic conductivity field in the one-dimensional problem. In the present study, the dimensionless arithmetic mean of hydraulic conductivity is taken as unity. For the deterministic and homogeneous case, the value of hydraulic conductivity is also taken as unity. For cases 1E and 1F the effective value hydraulic conductivity become less than unity. For flow through one-dimensional column with heterogeneous hydraulic conductivity field, the effective value of hydraulic conductivity is essentially the harmonic mean [*Gelhar,* 1993, p. 110], which is lesser than the arithmetic mean. It can be shown analytically that the effective flow velocity and its standard deviation are functions of the mean and variance of the hydraulic conductivity as well as the ratio of the length of the column to the correlation length. The uncertainty of flow velocity increases with the variance of the hydraulic conductivity. It is higher for smaller ratios of length of the column to the correlation length. Under these conditions, the uncertainty of concentration increases if the correlation length of the

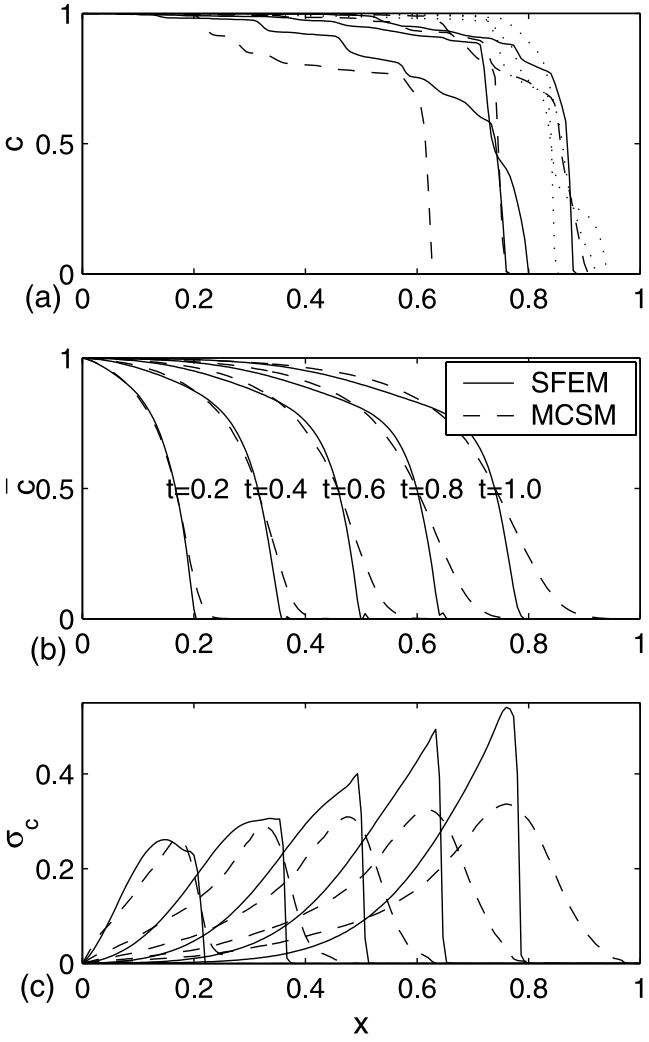

Figure 4. Concentration plot for case 1D. (a) Realizations generated using MCSM for time $t = 1.0$, (b) comparison of mean concentration between SFEM and MCSM at different time, and (c) comparison standard deviation of concentration between SFEM and MCSM.

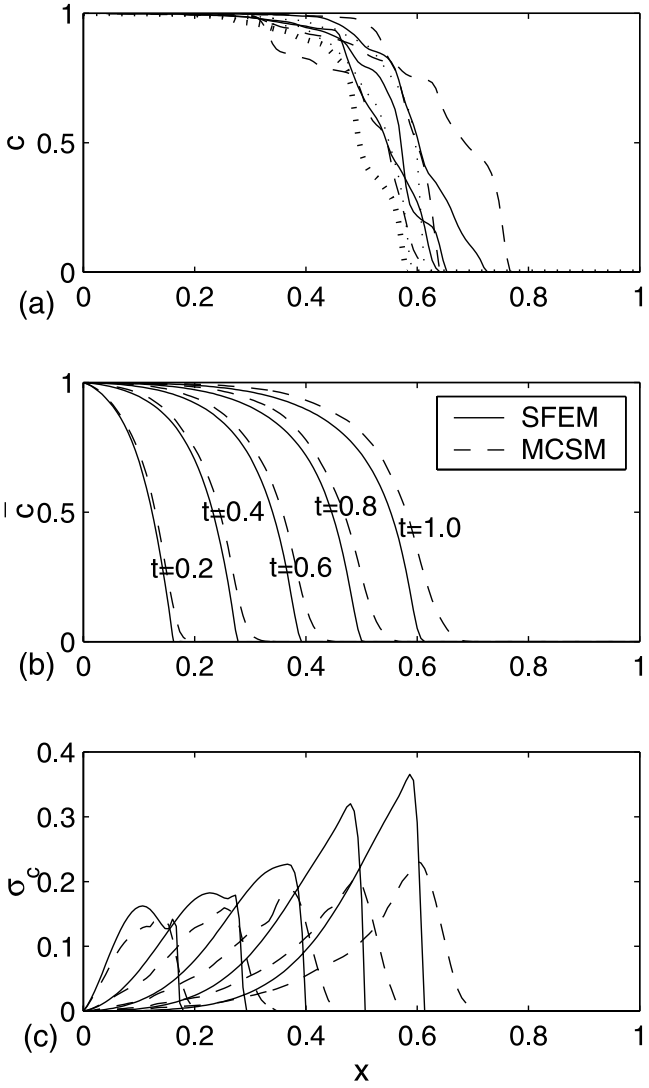

Figure 5. Concentration plot for case 1E. (a) Realizations generated using MCSM for time $t = 1.0$, (b) comparison of mean concentration between SFEM and MCSM at different time, and (c) comparison standard deviation of concentration between SFEM and MCSM.

hydraulic conductivity is chosen larger compared with that of other random parameters as shown for the case 1F. If the size of column is taken larger for the flow simulation, the variance of the flow velocity will reduce and the results obtained by SFEM for higher correlation length cases would show good matching with MCSM results.

[19] The accuracy in the results obtained from SFEM are quantified by comparing with MCSM using the following error norms for mean and standard deviation in concentration.

$$\text{Error}_{\bar{c}} = \frac{1}{N_c}\sum_{i=1}^{N_c}\frac{|\bar{c}_{i\text{SFEM}} - \bar{c}_{i\text{MCSM}}|}{\bar{c}_{i\text{MCSM}}}, \tag{37}$$

$$\text{Error}_{\sigma_c} = \frac{1}{N_c}\sum_{i=1}^{N_c}\frac{|\sigma_{c_i\text{SFEM}} - \sigma_{c_i\text{MCSM}}|}{\sigma_{c_i\text{MCSM}}}. \tag{38}$$

Here N_c is defined as the total number of nodes where $\bar{c} > 0.01$. Nodes corresponding to mean concentration ($\bar{c} \leq 0.01$) are neglected in the computations of the above error norms because the objective is to assess the comparison between the methods at locations with reasonable mean concentrations. The plot of errors in mean and standard deviation of concentrations for cases 1A–1F at various time steps are shown in Figure 7.

[20] Higher coefficient of variation results in a larger error both in the mean and the standard deviations as expected for cases 1A–1D. The errors in the standard deviation are relatively higher than that of the mean since the SFEM uses a first-order accurate solution for the standard deviation while a second-order accurate solution for the mean. The error in the mean concentration is found to be approximately constant with time. The error in the mean concentration for the higher COV case (i.e., $\sigma_{f_n} = 0.85$

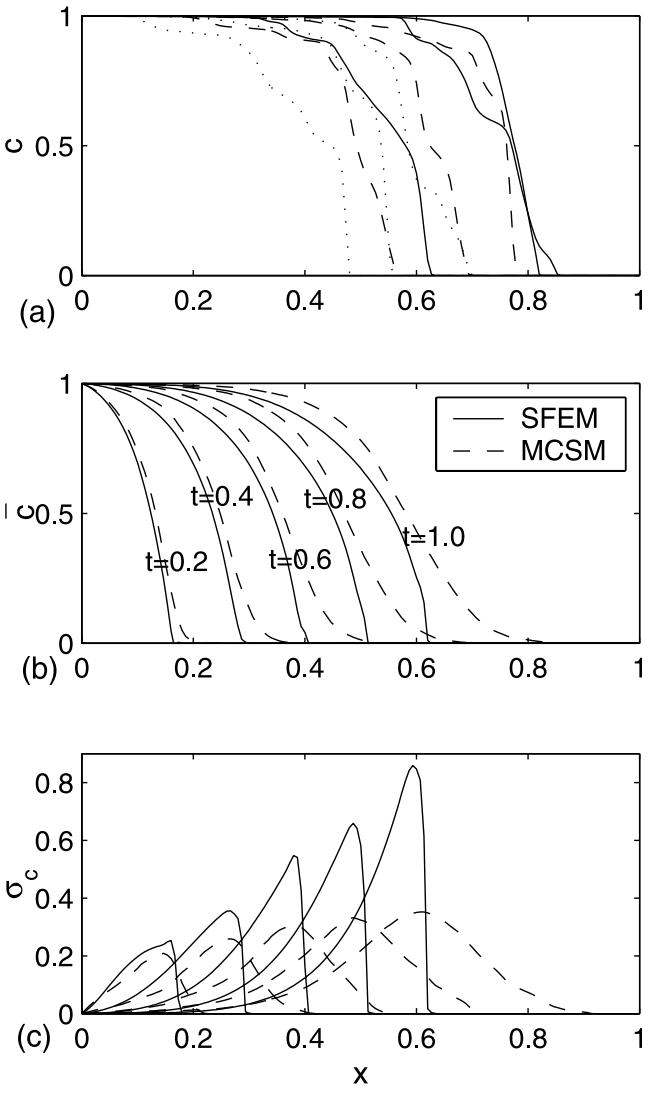

Figure 6. Concentration plot for case 1F. (a) Realizations generated using MCSM for time $t = 1.0$, (b) comparison of mean concentration between SFEM and MCSM at different time, and (c) comparison standard deviation of concentration between SFEM and MCSM.

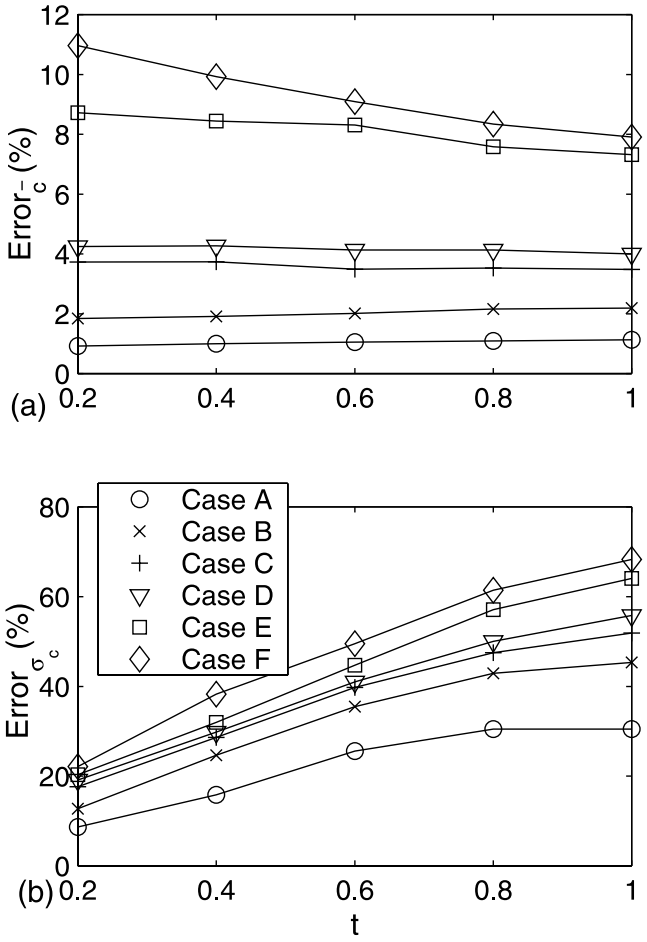

Figure 7. Temporal plot of error in (a) mean and (b) standard deviation of concentration obtained by SFEM for different cases A–E in the one-dimensional problem.

corresponding to case 1D) is found to be less than 5%. The error in the standard deviation of concentration (Figure 7b) increases with time (size of the plume) and is found to reach a steady state. For the higher COV case (case 1D) the error is found to be approximately 55%. It is observed that at upstream locations of the concentration front, the steady state mean and standard deviation of concentration by SFEM match better with MCSM. The error of both the mean and variance is found to be higher when the hydraulic conductivity is also considered as a random field (cases 1E and 1F) even though the COV used is 0.5 ($\sigma_{f_k} = 0.48$). The computational time required for SFEM is approximately equal to the time required to perform 10 realizations in the MCSM for the one-dimensional problem.

6.2. Three Dimensional Problem

[21] The SFEM developed in section 4 is applied for studying the probabilistic behavior of concentration distribution in a three-dimensional problem setting as shown in Figure 8. In this problem, the hydraulic conductivity, porosity, decay coefficient, dispersivity, and molecular diffusion are considered as spatially varying random fields and are positively correlated. The random sorption coefficient is assumed to have negative correlation with the rest of the other random parameters. Further, the correlation length along the horizontal plane are assumed to be same (i.e., $\lambda_1 = \lambda_2 = \lambda_h$), while the horizontal correlation length (λ_h) is considered larger in comparison to that of the vertical direction (λ_3). The flow field in this problem becomes nonuniform because of the constant continuous recharge from the pollutant source combined with the lateral groundwater flow in the underlying permeable layer.

[22] The mean and covariance of the random flow field is derived from the random hydraulic conductivity field. Along with covariance matrices of the other random fields, the covariance of velocity is also used for the probabilistic

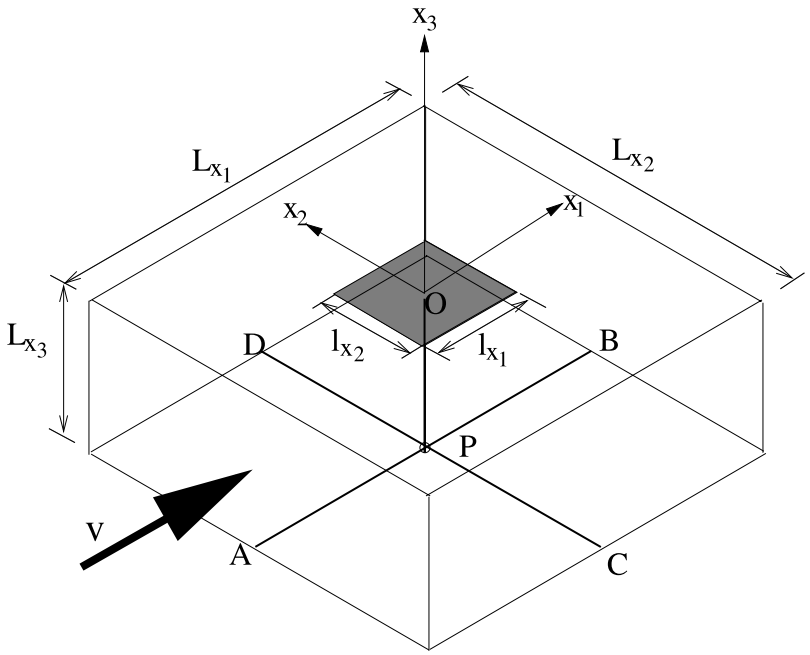

Figure 8. A schematic diagram of three-dimensional problem with continuous source at the top.

Table 2. Coefficients of Variation of Random Properties for Various Cases

Case	$\rho_{\{K,\gamma d,\alpha,D\mathrm{m}\}}$	λ_h^K	λ_v^K	$\rho_{\{K,n\}}$	λ_h^n	λ_v^n	$\rho_{\{K,k_d\}}$	λ_h^{kd}	λ_v^{kd}
3A	1	1.00	0.50	1	1.00	0.50	−1	1.00	0.50
3B	1	1.00	0.50	0	2.00	1.00	0	0.50	0.25

analysis of contaminant transport. A square contaminant source of dimension $l_{x_1} = l_{x_2} = l$ is assumed to be located above the permeable layer. The governing equation (1), the boundary conditions in section (2), and the properties are made dimensionless with respect to the depth of the permeable layer (h) and the horizontal pore water velocity for a deterministic case without any recharge (v_d). Here $c(\mathbf{x}, t) = \tilde{c}(\tilde{\mathbf{x}}, \tilde{t}) / c_0$ is the dimensionless concentration of the pollutant at a dimensionless distance $\mathbf{x} = \tilde{\mathbf{x}} / h$ at the dimensionless time ($t = v_d\tilde{t} / h$). Here c_0 is the concentration at the top of the soil. Further, $v(\mathbf{x}) = \tilde{v}(\tilde{\mathbf{x}}) / v_d$, $\alpha(\mathbf{x}) = \tilde{\alpha}(\tilde{\mathbf{x}}) / h$, $D_{\mathrm{m}}(\mathbf{x}) = \tilde{D}_{\mathrm{m}}(\tilde{\mathbf{x}}) / (v_d h)$, $\gamma_d(\mathbf{x}) = \tilde{\gamma}_d(\tilde{\mathbf{x}})h / v_d$, and $q = \tilde{q} / v_d$ are the dimensionless velocity of flow, dispersivity, molecular diffusion, decay coefficient, and recharge at the top, respectively. The following numerical values of properties are used for solving the three-dimensional problem: $l = 0.5$, $\overline{n} = 0.4$, $\overline{k}_d = 0.2$, $\overline{\gamma}_d = 0.2$, $\overline{\alpha} = 0.2$, $\overline{D}_m = 0.5$, and $q = 0.5$. For the three-dimensional simulation, the coefficient of variation of the random properties are taken as, $\mathrm{COV}_K = 1.0$ (σ_{f_K}=0.803), $\mathrm{COV}_n = 0.4$ (σ_{f_n}=0.309), $\mathrm{COV}_{k_d} = 0.4$, $\mathrm{COV}_{\gamma_d} = 0.4$, $\mathrm{COV}_{\alpha} = 0.4$, $\mathrm{COV}_{D_{\mathrm{m}}} = 0.4$. The standard deviation of log hydraulic conductivity used in this study corresponds to mild heterogeneity of the porous medium based on the values reported for various field investigations [*Gelhar*, 1993, pp. 291–292]. Further, the $\sigma_{f_K} = 0.803$ used is in the range of various investigations made using numerical methods. The dimensionless domain size for the three-dimensional problem is $5 \times 4 \times 1$. For this three-dimensional transport problem, the numerical grid Peclet number is kept close to 0.5.

[23] To check the accuracy of results and computational efficiency of the SFEM, the probabilistic analysis has been carried out by commonly used MCSM (1000 realizations) for $B = 67.9$ and $\lambda = 0.5$. Figure 9 demonstrates the comparison of temporal behavior of mean and standard deviation of concentration at location P (shown in Figure 8). In Figure 9a, the mean break through curve obtained by SFEM shows sharpness than that of the MCSM. Similar pattern is also observed for the mean concentration in the one-dimensional problem as well. Figure 9b shows peaks in the temporal plot of the standard deviation concentration obtained by both SFEM and MCSM. However, MCSM produces a lower peak and higher spread in comparison to the SFEM. Since the arrival time of the concentration front varies from one realization to another realization in the MCSM, this might result in a higher spread or dispersion and accordingly produces a lower peak for the ensemble averages of the concentration at any location. The proposed SFEM exhibits oscillations in the simulations of the statistical moments of the concentration. This is due to the second-order term in the mean concentration. This behavior is observed mainly at the tail end regions of the concentration fronts where concentrations being very small (close to zero), the combination of the zeroth-order and second-order terms results in negative values. Further, the oscillation and the negative values are noted during the early stages of concentration break through curve at any location. Similar behavior was also reported by *Morales-Casique et al.* [2006]. The effect of the oscillation of the second-order is more pronounced for a stronger heterogeneous and nonlinear case. The inclusion of higher-order terms may improve the results.

[24] The contour plot of mean and coefficient of variation of concentration at dimensionless time ($t = 16$) along the planes $x_2 = 0$ and $x_1 = 0$ which are obtained by SFEM are compared with MCSM in Figure 10. The contours of the mean concentration as shown in Figures 10a and 10b are matching quite well overall for the two methods. A marginal variation between them is observed for the results along downstream flow direction. The contours COV of concentration (Figures 10c and 10d) obtained by SFEM are found to be marginally shifted along the upstream direction and spread higher compared to MCSM. The convergence of the solution error with size of the sample for MCSM is demonstrated in Figure 11. It is observed that for this problem, the solutions with MCSM are stable for 1000 realizations, and the maximum error for this case between MCSM and SFEM is less than 10%. The relatively lower error for the three-dimensional problem in comparison to the one-dimensional problem discussed earlier could be attributed because of several reasons. Some of these could be (1) the choice of higher decay coefficient used in this problem, which limits the spread of the plume thereby the resulting lesser effect of spatial variability of parameters and (2) the dispersion process in three-dimensional problem plays an important role in reducing the uncertainty in the concentration and hence correspondingly the error. Further, the relative effects of boundary and plume size on the uncertainty and corresponding error are discussed at the end of this section.

[25] The computational time required for the solution of the three-dimensional problem by SFEM, which uses 910 grids, is 3050 s while for MCSM (with 1000 realizations) is 65,800 s on COMPAQ Alpha Server ES40 (a cluster of four CPUs with 667 MHz). This indicates that the time required for one simulation run by SFEM for the three-dimensional problem is approximately equal to the time required for five realizations with MCSM. This higher computational efficiency with SFEM is very useful when performing simulations for problems involving larger domain sizes and finer grids.

[26] The behavior of mean and standard deviation of concentration for variation in the affinity parameters (B) and different correlation cases of the random parameters are studied by SFEM using finer grid in the three-dimensional problem. The correlation cases are presented in Table 2. In case 3A, the parameters are perfectly correlated and have same correlation lengths. In case 3B, the correlation lengths of porosity field are taken twice of that of conductivity since its variability in geologic media may show long range correlation [*Hewett*, 1986]. In case 3B, sorption coefficient is also considered to be uncorrelated with the rest of all other random parameters. The correlation lengths of sorption coefficient field are taken as half of that of hydraulic conductivity field.

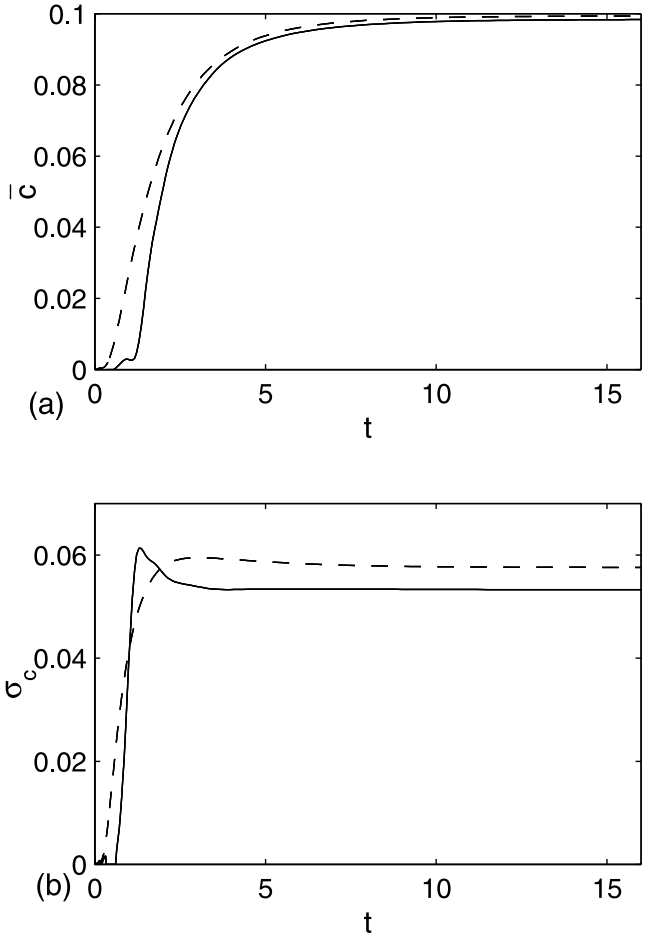

Figure 9. Comparison of mean and standard deviation of concentration obtained by SFEM (straight line) and MCSM (broken line) at location P below the source for the three-dimensional problem.

[27] The mean concentration increases monotonically with time and reaches a steady state value for different cases as shown in Figure 12a. The standard deviation of concentration also increases monotonically with time and reaches a steady state. For a higher value of B and perfectly correlated case (case 3A), it shows a peak before reaching a lower steady state as shown in Figure 12b. The mean concentrations are found to be higher for lower values of B, while the standard deviation of concentrations are found to be vice-a-versa. Comparison of results for two different correlation cases (cases 3A and 3B) show that the mean concentration is not affected much, but standard deviation of concentration is lower for uncorrelated case with different correlation lengths (case 3B). At large dimensionless time (t = 16), when the concentration in most part of the domain reaches a steady state because of first-order decay, the mean concentration decreases with distance from the source as shown in the contour plots in the Figures 13a, 13b, 14a, and 14b. But the prediction uncertainty in terms of coefficient of variation of concentration is found to increase with distance from the source as shown in Figures 13c, 13d, 14c, and 14d. This result is expected, as the uncertainty is lower close to the deterministic source. The coefficient of variation is found to be higher for fully correlated case (case 3A). The COV of concentration is found to be higher for a larger B. The results indicate that when the nonlinearity in the sorption isotherm is higher, at the steady state, the spreading of the concentration plume of the decaying solute is smaller but the prediction uncertainty increases with the increase in the sorption nonlinearity. The computational time required for the solution for each case of the three-dimensional problem, which uses 1728 grids, is 87,200 s (approximately 1 day) on COMPAQ Alpha Server ES40 (a cluster of four CPUs with 667 MHz).

[28] The deterministic boundary condition and size of the domain with respect to the correlation length affect the spatial distribution of (ensemble) moments of flow (i.e., mean and covariances of flow velocity). Because of heterogeneity, the effective mean velocity vector alters, which depends on the ratio of size of the domain to the correlation length. Similar to one-dimensional problem, it is known that for three-dimensional problem also the standard deviation of the longitudinal component of flow velocity decreases with the increase in the ratio. This implies that if the size of domain used is larger for the simulation of steady state flow, the uncertainty of the velocity may reduce. Because of the coupling of flow and transport equations, both mean and covariances of concentration are affected by the physical setting of the flow problem. The accuracy of results by SFEM also depends on the physical setting of the flow problem. This aspect has been mentioned in one-dimensional problem (for cases 1E and 1F) wherein the effects of length of column and correlation length have been discussed. Hence the larger domain size for flow simulation results in a lower standard deviation of velocity and thus a lower uncertainty in the concentration prediction. In such circumstances, SFEM may perform better since the variance of velocity, which is the key input parameter, is small. But the boundary conditions for the transport problem directly affect the spatial and temporal variation of the mean concentration. This effect is very similar to the deterministic case. For the stochastic case the standard deviation increases with the ratio of the size of the plume as shown for the one-dimensional problem. It is observed that for both the one- and three-dimensional problems, the standard deviation is very high at the tail end of the plume (where the concentrations are very low), correspondingly, the error with SFEM is also high at these locations.

7. Conclusions

[29] In the present study, a computationally efficient SFEM has been developed for solving the nonlinear problems pertaining to the transport of solutes in three-dimensional heterogeneous porous media. The method is based on the classical perturbation-based approach and is second-order accurate in mean and first-order accurate in the standard deviation. Because of the nonlinear governing equations, the method has to be combined with an iterative approach to solve the nonlinear algebraic equations discretized using finite element method.

[30] The method is applied for the probabilistic analysis of a nonlinearly sorbing solute while undergoing transport in porous media and tested for its accuracy while comparing with the MCSM. As the computational cost of SFEM increases with the increase in the number of random parameters and in addition it may have lesser accuracy with

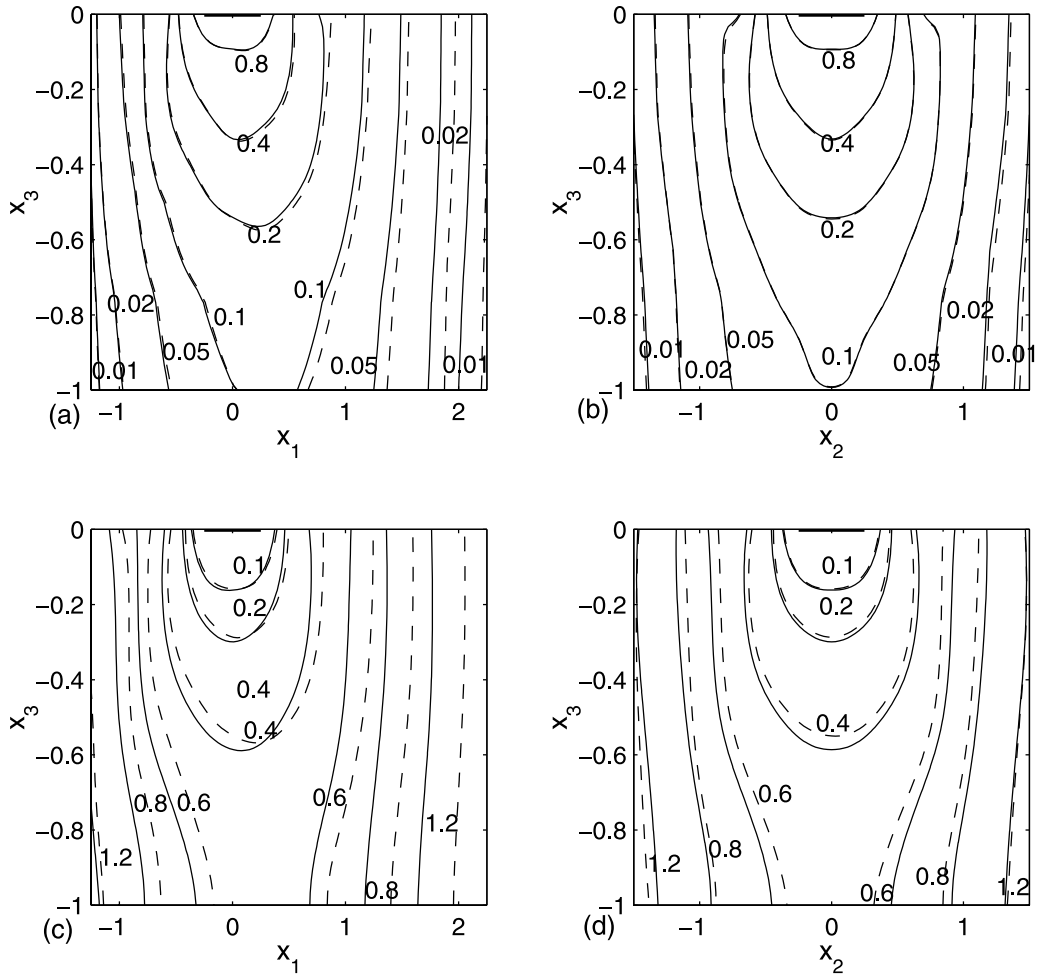

Figure 10. Comparison of mean and coefficient of variation of concentration at $t = 16$ for $B = 67.9$ and $\lambda_h = 0.5$ in the three-dimensional problem obtained by SEFM (straight line) and MCSM (broken line). Mean concentration (a) along the ($x_2 = 0$) plane and (b) along the ($x_1 = 0$) plane, coefficient of variation (c) along the ($x_2 = 0$) plane and (d) along the ($x_1 = 0$) plane.

multiple random parameters, in this study, performance of SFEM is investigated with multiple random parameters. The analyses are carried out for both one- and three-dimensional problems considering hydraulic conductivity, porosity, dispersivity, diffusion coefficient, sorption coefficient, and decay coefficient as random fields. In the one-dimensional transport problem with continuous source, the mean concentration breakthrough curves at various time steps as obtained by SFEM are found to have sharp fronts, and their spread does not increase with time as expected for the case of a nonlinear sorption problem. On the other hand, MCSM results show that the mean concentration has a dispersive front behavior, which increases with time. The standard deviation is found to be the highest at the concentration front location. At the front location, the mean and standard deviation of concentration by SFEM when compared with MCSM are found to have higher deviations. A comparison of the results between SFEM and MCSM for the three-dimensional problem (break through curve and contour plots) indicates that results of SFEM match quite well for mild heterogeneity cases with 0.85 as the upper limit of standard deviation of log hydraulic conductivity (coefficient of variation of hydraulic conductivity being 1.0). The error with SFEM for the mean and standard deviation of concentration is found to be less than 10% for the three-dimensional problem setting. The prediction uncertainty and, correspondingly, the error with SFEM may depend on the boundary conditions, the size of the domain, and the plume size. The variation of the flow decreases with increase in the size of the domain. In such circumstances, the prediction uncertainty of the concentrations is lower, and the SFEM would result in lesser error. But as the mean and the standard deviation of concentration obtained by SFEM at the tail end of the plume have higher deviations when compared with MCSM, the overall error increases slowly with the size of the plume.

[31] The larger value of sorption affinity parameter results in a higher nonlinearity in the sorption isotherm and causes more retardation to the solute transport. At the steady state, the size of the plume of the decaying solute is smaller for a larger value of the sorption affinity parameter. But the coefficient of variation of the concentration is more for a higher nonlinear case. The results for both perfectly correlated case (case 3A) and uncorrelated case with different

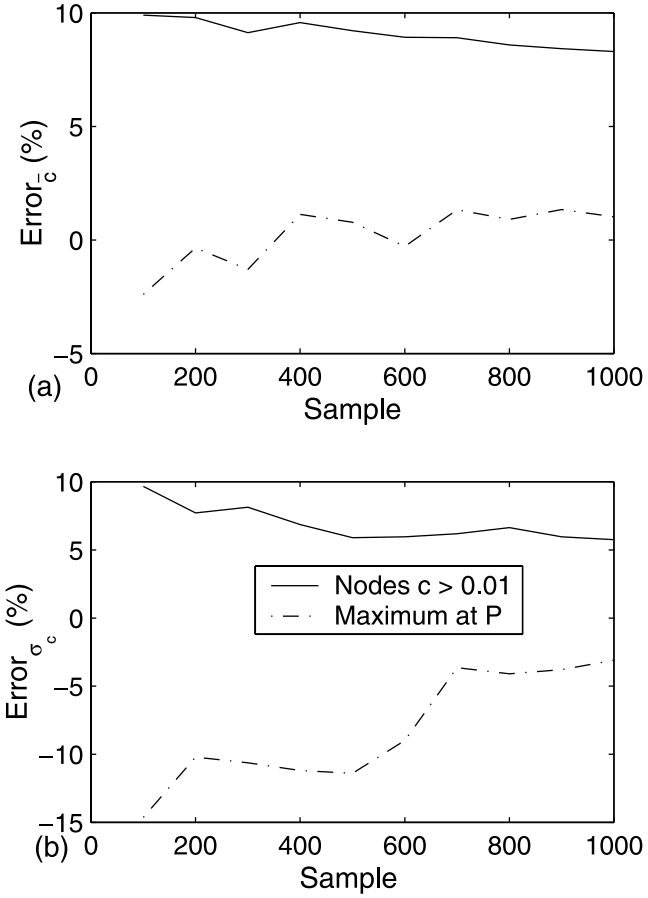

Figure 11. Convergence of error with sample size in the MCSM for the three-dimensional problem.

correlation length (case 3B) are qualitatively similar. Sensitivity studies with varying correlation length among the random parameters indicate that the patterns of the mean and the standard deviation of concentration are quite similar. A perfectly correlated case produces a higher prediction uncertainty than the uncorrelated case. The comparison between the computational time required for SFEM and MCSM based on the one- and three-dimensional problems suggests that the SFEM is very efficient. The proposed SFEM holds good for low-variance cases corresponding to mild heterogeneity of governing parameters as it uses only up to second-order terms in the Taylor series approximation. The SFEM in the present study is tested with simpler numerical test cases for the nonlinear solute transport problem. The results are encouraging to use this method for complicated test problems, which may require following adaptations with this method.

[32] For the transport of solutes in field applications, the Peclet number varies in a wide range from 10^{-1} to 10^{4}. As it is based on a standard Galerkin finite element method, it is applicable for only dispersion-dominated problems (i.e., not applicable for higher Peclet numbers). By using finite element formulations developed and available for advection dominated problems, one can develop a SFEM for both advection and dispersion dominated cases.

[33] The proposed SFEM method can be easily used for conditional stochastic simulation of flow and solute transport in heterogeneous porous medium. In general, the conditioning is done to the measurement of the governing parameters as well as the state variables (or the dependent variables). For the first case, the conditional mean of the random vector (discretized random field of the governing parameters) and conditional covariance matrix can be derived using various methods such as Kriging, triangular decomposition method, or eigen value decomposition. The conditional mean and variance of the random space function are not constant even though the random parameter is initially assumed to be statistically homogeneous since at the locations where the values are known, the parameter is considered to be deterministic and the variance is set to be zero. Being a numerical method, SFEM can directly use the conditional mean and the covariance for conditional stochastic simulation. For the second case, the conditional stochastic analysis based on the measurements of state variable can be performed by coupling the SFEM with a suitable optimization technique [*Hernandez et al.*, 2003, 2006]. The sensitivity analysis, which is inherent in the SFEM approach, can be used for the optimization also. In an alternative way, the conditioning to the temporal

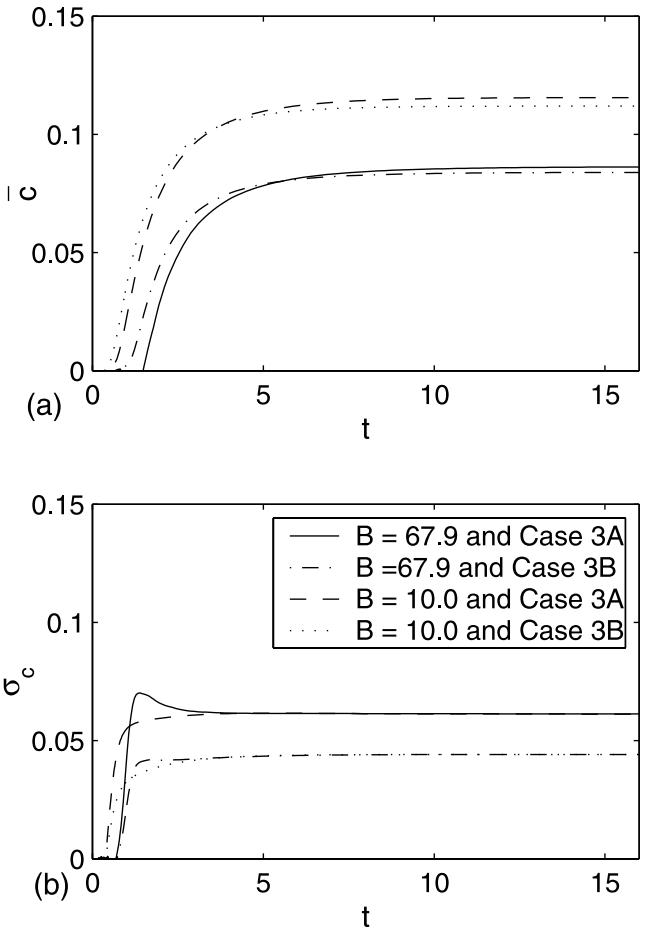

Figure 12. The effect of affinity parameter (B) and correlation length (λ_h) on the mean and standard deviation of concentration at location P below the source for the three-dimensional problem.

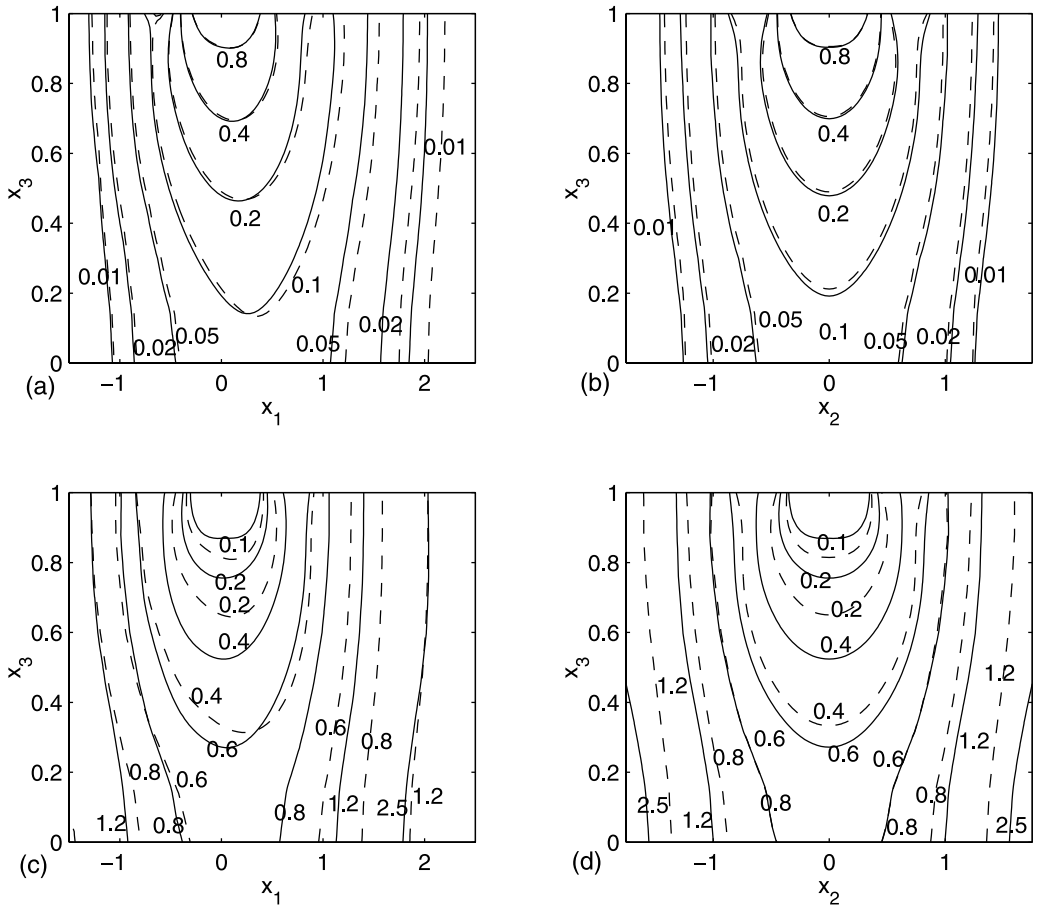

Figure 13. Contour plots of distribution of mean concentration and coefficient of variation at $t = 16$ for $B = 67.9$ in the three-dimensional problem. Mean concentration (a) along the ($x_2 = 0$) plane and (b) along the ($x_1 = 0$) plane, coefficient of variation (c) along the ($x_2 = 0$) plane and (d) along the ($x_1 = 0$) plane. Straight line represents case 3A, and broken line represents case 3B.

measurements of the state variable at few locations can be performed by treating the measurements as constraints to the finite element formulation. These constraints can be incorporated into the global matrix and the right hand side vector in a similar way as is done for the boundary conditions.

[34] Several field experimental results show that the statistical parameters (for example, mean, variance, correlation lengths, etc.) vary within a range. This implies that the random function representing the parametric spatial variation is not stationary. In such circumstances, the SFEM can be a very good alternative tool for the probabilistic analysis of solute transport problem in such complicated heterogeneous media, if suitably combined with a proper method of constructing the covariance matrix.

Appendix A: Mean and Covariance of Velocity and Dispersion Coefficient

[35] Similar to the transport, the global equation for flow for a given head and flux boundary conditions is expressed as,

$$[K]\{H\} = \{H_0\}. \tag{A1}$$

Here $[K]$ is the global hydraulic conductivity matrix in the flow equation. The ith component of seepage flux of pth element is obtained by taking average of that at all the Gauss points ($\mathbf{x}_k$, for $k = 1, \cdots, N_G$, where N_G is the number of Gauss points) and is given as,

$$q_{i_p} = -\frac{1}{N_G} K_{ij_p} \sum_{k=1}^{N_G} \frac{\partial N_l(\mathbf{x})}{\partial x_j}\Big|_{\mathbf{x}_k} H_l = -\frac{1}{N_G} K_p \sum_{k=1}^{N_G} \frac{\partial N_l(\mathbf{x})}{\partial x_i}\Big|_{\mathbf{x}_k} H_l. \tag{A2}$$

For isotropic cases, the hydraulic conductivity tensor becomes a scalar quantity (K_p).

[36] Using the similar methodology presented for the transport problem (section 4), the perturbation approach can also be applied on the flow equation (A1), to obtain the mean and random perturbed components of the hydraulic head. In the case of the flow problem, the random properties are only the hydraulic conductivities of the elements K_p, ($p = 1, 2. \cdots, N$), and hence the mean and the random component of the hydraulic head are expressed as,

$$\{\overline{H}\} = \left([I] + \sum_{p=1}^{N_k} \sum_{q=1}^{N_k} [\overline{K}]^{-1} [K]^{(I)}_{K_p} [\overline{K}]^{-1} \cdot [K]^{(I)}_{K_q} \overline{K'_p K'_q} \right) [\overline{K}]^{-1} \{H_0\}, \tag{A3}$$

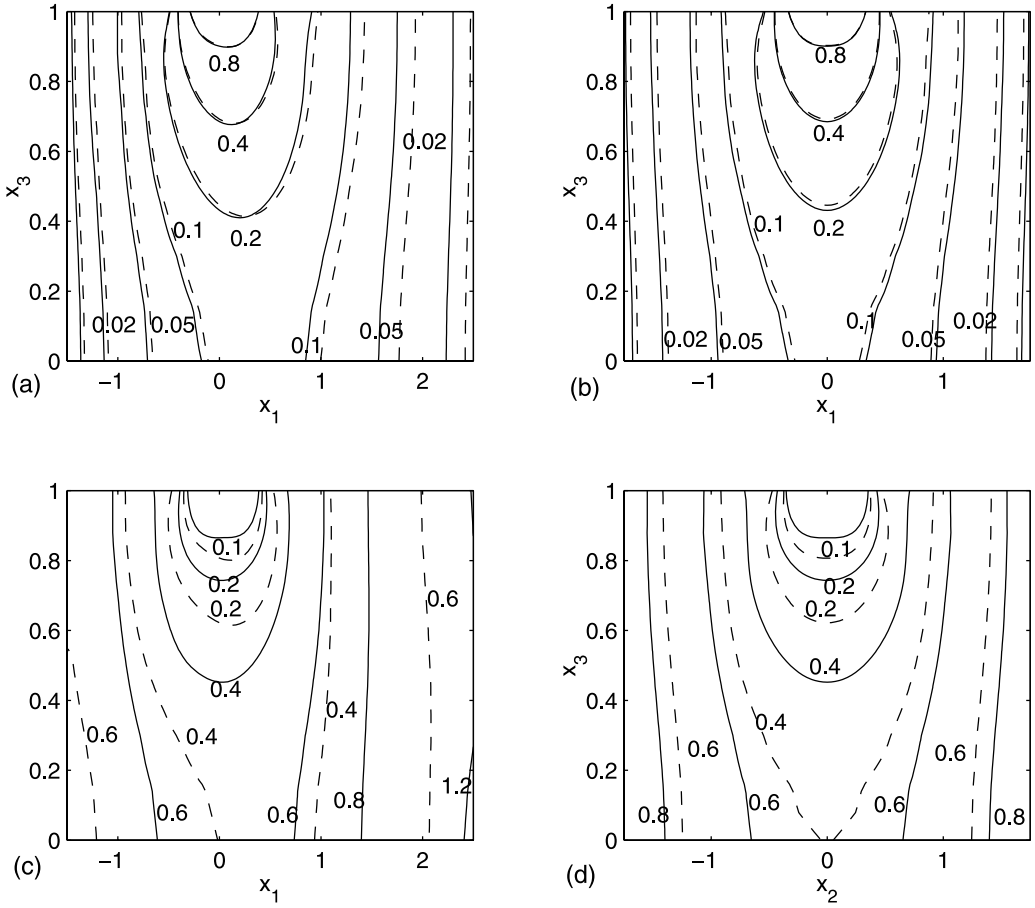

Figure 14. Contour plots of distribution of mean concentration and coefficient of variation at $t = 16$ for $B = 10.0$ in the three-dimensional problem. Mean concentration (a) along the ($x_2 = 0$) plane and (b) along the ($x_1 = 0$) plane, coefficient of variation (c) along the ($x_2 = 0$) plane and (d) along the ($x_1 = 0$) plane. Straight line represents case 3A, and broken line represents case 3B.

$$\{H\}' = \sum_{p=1}^{N_k} \{H\}_{K_p}^{(I)} K_p' \quad \text{where } \{H\}_{K_p}^{(I)} = -\left[\overline{K}\right]^{-1}[K]_{K_p}^{(I)}\left[\overline{K}\right]^{-1}\{H_0\}. \tag{A4}$$

Using equations (A3) and (A4), the mean and random component of seepage flux (q_{i_p}) are written as,

$$\overline{q}_{ip} = -\frac{1}{N_G}\sum_{k=1}^{N_G}\left.\frac{\partial N_l(\mathbf{x})}{\partial x_i}\right|_{\mathbf{x}_k}\left(\overline{K}_p\overline{H}_l + \sum_{q=1}^{N_k} H_{l,K_q}^{(I)}\overline{K_p'K_q'}\right), \tag{A5}$$

$$q_{ip}' = -\sum_{q=1}^{N_k}\frac{1}{N_G}\sum_{k=1}^{N_G}\left.\frac{\partial N_l(\mathbf{x})}{\partial x_i}\right|_{\mathbf{x}_k}\left(\overline{H}_l\delta_{pq} + \overline{K}_p H_{l,K_q}^{(I)}\right)K_q' = \sum_{q=1}^{N_k} q_{ip,K_q}^{(I)} K_q'. \tag{A6}$$

From the above expression, one can obtain the auto covariance of seepage flux and cross covariance with any other random properties (r_j') using the auto covariance of hydraulic conductivity and cross covariance of hydraulic conductivity with r_j', which may be given as,

$$\overline{q_{ip_1}'q_{jp_2}'} = \sum_{q_1=1}^{N_k}\sum_{q_2=1}^{N_k} q_{ip_1,K_{q_1}}^{(I)} q_{jp_2,K_{q_2}}^{(I)}\overline{K_{q_1}'K_{q_2}'} \text{ and } \overline{q_{ip}'r_j'} = \sum_{q=1}^{N_k} q_{ip,K_q}^{(I)}.\overline{K_q'r_j'} \tag{A7}$$

$\overline{q}_{ip}$ and q_{ip}' are the mean and the random component, respectively, of the product $n_p v_{i_p}$ in equation (9). The product $n_p D_{ij_p}$ can be written in terms of water flux and is expressed as,

$$n_p D_{ij_p} = \alpha_p\left((1-\epsilon)\frac{q_{ip}q_{jp}}{q_p} + \epsilon q_p\delta_{ij}\right) + n_p D_{\mathrm{m}p}\delta_{ij} \tag{A8}$$

The mean of the resultant seepage flux ($q_p = (\sum_{i=1}^{3} q_{i_p}{}^2)^{1/2}$), and its random component are expressed as,

$$\overline{q}_p = q_p + \frac{1}{q_p}\sum_{i=1}^{3} C_{q_{ip}q_{ip}} - \frac{1}{q_p^3}\sum_{i=1}^{3}\sum_{j=1}^{3}\overline{q}_{ip}\overline{q}_{jp}C_{q_{ip}q_{jp}} \text{ and } q_p' = \frac{1}{q_p}\sum_{i=1}^{3}\overline{q}_{ip}q_{ip}'. \tag{A9}$$

The effective mean dispersion coefficient and its random component are obtained by using equation (5), along with the expression (A9), which may be expressed as,

$$\overline{n_p D_{ij_p}} = \left(\overline{\alpha}_p \left(\frac{\overline{q}_{ip}\overline{q}_{j_p} + C_{q_{ip}q_{j_p}}}{\overline{q}_p} - \frac{\overline{q}_{ip}C_{q_{j_p}q_p} + \overline{q}_{j_p}C_{q_{ip}q_p}}{\overline{q}_p^2} + \frac{\overline{q}_{ip}\overline{q}_{j_p}C_{q_pq_p}}{\overline{q}_p^3}\right) + \frac{\overline{q}_{ip}C_{q_{j_p}\alpha_p} + \overline{q}_{j_p}C_{q_{ip}\alpha_p}}{\overline{q}_p} - \frac{\overline{q}_{ip}\overline{q}_{j_p}C_{q_p\alpha_p}}{\overline{q}_p^2}\right)(1-\epsilon) + \epsilon\left(\overline{\alpha}_p\overline{q}_p + C_{q_p\alpha_p}\right)\delta_{ij} + \left(\overline{n}_p\overline{D}_{mp} + C_{n_pD_{mp}}\right)\delta_{ij} \text{ and} \tag{A10}$$

$$\left(n_p D_{ij_p}\right)' = \left(\overline{\alpha}_p\left(\frac{\overline{q}_{ip}q'_{j_p} + \overline{q}_{j_p}q'_{ip}}{\overline{q}_p} - \frac{\overline{q}_{ip}\overline{q}_{j_p}q'_p}{\overline{q}_p^2}\right) + \alpha'_p\frac{\overline{q}_{ip}\overline{q}_{j_p}}{\overline{v}_p}\right) \cdot (1-\epsilon) + \epsilon\left(\overline{\alpha}_p q'_p + \alpha'_p\overline{q}_p\right)\delta_{ij} + \left(\overline{n}_p D'_{mp} + n'_p\overline{D}_{mp}\right)\delta_{ij}. \tag{A11}$$

Notation

$c(\mathbf{x}, t)$	Concentration in aqueous phase
$s(\mathbf{x}, t)$	Concentration in sorbed phase
$g(\mathbf{x}, t)$	Nonlinear reaction function
$\mathbf{x}$ and t	Position vector and time, respectively
$n(\mathbf{x})$	Porosity
$\mathbf{v}(\mathbf{x})$	Velocity vector of flow
$\mathbf{D}(\mathbf{x})$	Hydrodynamic dispersion coefficient tensor
$k_d(\mathbf{x})$	Sorption coefficient
ρ_b	Bulk density of soil
$\gamma_d(\mathbf{x})$	Decay coefficient
$\alpha(\mathbf{x})$	Local dispersivity
ϵ	Ratio of transverse to longitudinal dispersivity
$D_{\mathrm{m}}(\mathbf{x})$	Effective molecular diffusion coefficient
$c_0(\mathbf{x})$	Initial concentration in the domain Ω
$c_b(\mathbf{x}, t)$ and $f_b(\mathbf{x}, t)$	Specified concentration at boundary Γ_1 and solute flux at boundary Γ_2
n_{x_i}	Direction cosine of the normal with x_i axis
$\mathbf{q}(\mathbf{x})$	Water flux vector
$h(\mathbf{x})$	Hydraulic head
$\mathbf{K}(\mathbf{x})$	Hydraulic conductivity
$h_b(\mathbf{x}, t)$ and $q_b(\mathbf{x}, t)$	Specified hydraulic head at boundary $\Gamma^h{}_1$ and water flux at boundary $\Gamma_2{}^h$
$\cdot$	Time derivative
B	Sorption affinity parameter
m	An exponential parameter in Langmuir-Freundlich isotherm equation
$[R_c]$ and $[R_g]$	Coefficient matrix for time derivative of aqueous and sorbed concentration
$[D_c]$ and $[D_g]$	Coefficient matrix for aqueous and sorbed concentration
Δt	Time interval
θ	Fractional parameters for implicit time difference
$\{C^t\}$	Nodal aqueous concentration vector at time step t
$\{G^t\}$	Nodal sorbed concentration vector at time step t
$[D_1]$ and $[D_2]$	Coefficient matrix for aqueous concentration at present and previous time step
$[R_1]$ and $[R_2]$	Coefficient matrix for sorbed concentration at present and previous time step
$\{C_b{}^t\}$	Nodal source vector at time step t
$\{r\}$	Random vector due to random governing parameters
$\bar{}$	Mean
$'$	Random component
$[\mathrm{CV}]_{cc}$	Covariance matrix of aqueous concentration
σ_c	Standard deviation of aqueous concentration
$\{E^t\}$	A vector for the solution by Newton-Raphson method
$[\Delta E^t]$	Derivative matrix
$\{H\}$	Nodal hydraulic head vector
$[K]$	Coefficient matrix due to hydraulic head vector
λ_1, λ_2, and λ_3	Correlation lengths
σ_{f_K}, $\sigma_{f_{kd}}$, and σ_{f_n}	Standard deviation of log hydraulic conductivity, sorption coefficient, and porosity
$\tilde{}$	Dimensional quantity

[37] **Acknowledgments.** The authors thank particularly A. Guadagnini, the associate editor, for providing constructive and useful suggestions, which have helped in improving the manuscript at various stages. We also thank the anonymous reviewers for their helpful comments. The research grant awarded to the first author by the Indian Institute of Science, Bangalore, India, for carrying out this study is acknowledged.

References

Abulaban, A., and J. L. Nieber (2000), Modeling the effects of nonlinear equilibrium sorption on the transport of solute plumes in saturated heterogeneous porous media, *Adv. Water Resour.*, *23*, 893–905.

Allen-King, R. M., R. M. Halket, D. R. Gaylord, and M. J. L. Robin (1998), Characterizing the heterogeneity and correlation of perchloroethene sorption and hydraulic conductivity using a facies-based approach, *Water Resour. Res.*, *34*(3), 385–396.

Boving, T. B., and P. Grathwohl (2001), Tracer diffusion coefficients in sedimentary rocks: Correlation to porosity and hydraulic conductivity, *J. Contam. Hydrol.*, *53*, 85–100.

Berglund, S., and V. Cvetkovic (1996), Contaminant displacement in aquifers: Coupled effects of flow heterogeneity and nonlinear sorption, *Water Resour. Res.*, *32*, 23–32.

Bodin, J., F. Delay, and G. de Marsily (2003), Solute transport in a single fracture with negligible matrix permeability and: 2. Mathematical formalism, *Hydrol. J.*, *11*(4), 434–454.

Bosma, W. J. P., and S. E. A. T. M. van der Zee (1995), Dispersion of continuously injected, nonlinear adsorbing solute in chemically or physically heterogeneous porous formation, *J. Contam. Hydrol.*, *18*, 181–198.

Bosma, W. J. P., S. E. A. T. M. van der Zee, and C. J. van Duijn (1996), Plume development of a nonlinearly adsorbing solute in heterogeneous porous formation, *Water Resour. Res.*, *32*, 1569–1584.

Castillo-Cerda, C., X. Sanchez-Vila, L. Nunez-Calvet, and A. Guadagnini (2004), Conditional moments of residence time of sorbent solutes under radial flow, in Geostatistics for Environmental Applications, *Proc. of the fifth European Conference on Geostatistics for Environmental Applications*, edited by P. Renard, H. Demouget-Renard, and R. Froindevaux, 261–272, Springer, New York.

Chaudhuri, A., and M. Sekhar (2005a), Stochastic finite element method for probabilistic analysis of flow and transport in a 3-D heterogeneous porous formation, *Water Resour. Res.*, *41*, W09404, doi:10.1029/2004WR003844.

Chaudhuri, A., and M. Sekhar (2005b), Analytical solutions for macrodispersion in a 3D heterogeneous porous medium with random hydraulic conductivity and dispersivity, *Transp. Porous Media*, *58*, 217–241.

Cushman, J. H. (1997), *The Physics of Fluid in Hierarchical Porous Media: Angstroms to Miles*, Springer, New York.

Dagan, G. (1989), *Flow and Transport in Porous Formations*, Spinger, New York.

de Marsily, (1986), *Quantitative Hydrology: Groundwater Hydrology for Engineers*, Elsevier, New York.

Fernandez-Garcia, D., T. H. Illangaskare, and H. Rajaram (2005), Differences in the scale dependence of dispersivity estimated from temporal and spatial moments in physically and chemically heterogeneous porous media, *Adv. Water Resour.*, *28*, 745–759.

Garabedian, S. P., L. W. Gelhar, and M. A. Celia (1988), Large-scale dispersive transport in aquifers: field experiments and reactive transport theory, Rep. 315, Ralph M. Parsons Lab., Dep. of Civil Eng., Mass. Inst. of Technol., Cambridge.

Gelhar, L. W. (1993), *Stochastic Subsurface Hydrology*, Prentice-Hall, Upper Saddle River, N. J.

Gelhar, L. W., C. Welty, and K. R. Rehfeldt (1992), A critical review of data on field-scale dispersion in aquifers, *Water Resour. Res.*, *28*(7), 1955–1974.

Ghanem, R. (1998), Probabilistic characterization of transport in heterogeneous media, *Comput. Methods Appl. Mech. Eng.*, *158*, 199–220.

Guadagnini, A., and S. P. Neuman (1999), Nonlocal and localized analyses of conditional mean steady state flow in bounded, randomly nonuniform domains: 1. Theory and computational approach, *Water Resour. Res.*, *35*(10), 2999–3018.

Guadagnini, A., and S. P. Neuman (2001), Recursive conditional moment equations for advective transport in randomly heterogeneous velocity fields, *Transp. Porous Media*, *42*(1/2), 37–67.

Hassan, A. E. (2001), Water flow and solute mass flux in heterogeneous porous formations with spatially random porosity, *J. Hydrol.*, *242*, 1–25.

Hassan, A. E., J. H. Cushman, and J. W. Delleur (1998), A Monte Carlo assessment of Eulerian flow and transport perturbation models, *Water Resour. Res.*, *34*(5), 1143–1163.

Hernandez, A. F., S. P. Neuman, A. Guadagnini, and J. Carrera (2003), Conditioning mean steady state flow on hydraulic head and conductivity through geostatistical inversion, *Stochastic Environ. Res. Risk Assess.*, *17*(5), 329–338.

Hernandez, A. F., S. P. Neuman, A. Guadagnini, and J. Carrera (2006), Inverse stochastic moment analysis of steady state flow in randomly heterogeneous media, *Water Resour. Res.*, *42*, W05425, doi:10.1029/2005WR004449.

Hewett, T. A. (1986), Fractal distributions of reservoir heterogeneity and their influence on fluid transport, *SPE 15386 61st Annual Technical Conferences Society of Petroleum Engineering*, New Orleans, LA.

Hu, B. X., J. H. Cushman, and F. W. Deng (1997), Nonlocal reactive transport with physical, chemical and biological heterogeneity, *Adv. Water Resour.*, *20*, 293–308.

Huang, H., and B. H. Hu (2000), Nonlocal nonreactive transport in heterogeneous porous media with interregional mass diffusion, *Water Resour. Res.*, *36*(7), 1665–1675.

Kleiber, M., and T. D. Hien (1992), *The Stochastic Finite Element Method*, John Wiley, Hoboken, N. J.

Lichtner, P. C., and D. M. Tartakovsky (2003), Stochastic analysis of effective rate constant for heterogeneous reactions, *Stochastic Environ. Res. Risk Assess.*, *17*, 419–429.

Lie, Z., and C. Qui (2000), A stochastic variational formulation for nonlinear dynamic analysis of structure, *Comput. Methods Appl. Mech. Eng.*, *190*, 597–608.

Lu, Z., and D. Zhang (2004), A comparative study on uncertainty quantification for flow in randomly heterogeneous media using Monte Carlo simulations and conventional and KL-based moment-equation approaches, *SIAM J. Sci. Comput.*, *26*(2), 558–577.

Miralles-Wilhelm, F., and L. W. Gelhar (2000), Stochastic analysis of oxygen-limited biodegradation in heterogeneous aquifers with transient microbial dynamics, *J. Contam. Hydrol.*, *42*, 69–97.

Morales-Casique, E., S. P. Neuman, and A. Guadagnini (2006), Non-local and localized analyses of non-reactive solute transport in bounded randomly heterogeneous porous media: Computational analysis, *Adv. Water Resour.*, *29*, 1399–1418.

Ohlsson, Y., and I. Neretnieks (1995), Literature survey of matrix diffusion theory and of experiments and data including natural analogues, SKB TR 95-12, Swedish Nuclear Fuel Waste Management Co. Stockholm, Sweden.

Osnes, H., and H. P. Langtangen (1998), An efficient probabilistic finite element method for stochastic groundwater flow, *Adv. Water Resour.*, *22*(2), 185–195.

Perfect, E., M. C. Sukop, and G. R. Haszler (2002), Prediction of dispersivity for undisturbed soil columns from water retention parameters, *Soil Sci. Soc. Am. J.*, *66*, 696–701.

Rajaram, H. (1997), Time and scale-dependent effective retardation factors in heterogeneous aquifers, *Adv. Water Resour.*, *20*(4), 217–230.

Roberts, P. V., M. N. Goltz, and D. M. Mackay (1986), A natural gradient experiment on solute transport in a sand aquifer. 3. Retardation estimates and mass balance for organic solutes, *Water Resour. Res.*, *22*(13), 2047–2058.

Robin, M. J. L., E. A. Sudicky, R. Gillham, and R. G. Kachanoski (1991), Spatial variability of strontium distribution coefficients and their correlation with hydraulic conductivity in the Canadian Forces Base Borden aquifer, *Water Resour. Res.*, *27*(10), 2619–2632.

Sato, H. (1999), Matrix diffusion of simple cations, anions, neutral species in fractured crystalline rocks, *Nucl. Technol.*, *127*(2), 199–211.

Severino, G., G. Dagan, and C. J. van Duijn (2000), A note on transport of a pulse of nonlinearly reactive solute in a heterogeneous formation, *Comput. Geosci.*, *4*, 275–286.

Spanos, P. D., and R. Ghanem (1989), Stochastic finite element expansion for random media, *ASCE Eng. Mech.*, *115*(5), 1035–1053.

Strogatz, S. H. (1994), *Nonlinear Dynamics and Chaos: With Application to Physics, Biology, Chemistry, and Engineering*, Addison-Wesley, Boston, Mass.

Tang, D. H., and G. F. Pinder (1979), Analysis of mass transport with uncertain physical parameters, *Water Resour. Res.*, *15*(5), 1147–1153.

Vanmarcke, E. H. (1983), *Random Field Analysis and Synthesis*, MIT Press, Cambridge, Mass.

Wu, J., B. X. Hu, and C. He (2004), A numerical methods of moments for solute transport in a porous medium with multiscale physical and chemical heterogeneity, *Water Resour. Res.*, *40*, W01508, doi:10.1029/2002WR001473.

Xin, J., and D. Zhang (1998), Stochastic analysis of biodegradation fronts in one-dimensional heterogeneous porous media, *Adv. Water Res.*, *22*, 103–116.

A. Chaudhuri and M. Sekhar, Department of Civil Engineering, Indian Institute of Science Bangalore, Karnataka 560 012, India. (muddu@civil.iisc.ernet.inf)